Applied Catalysis B: Environmental 310 (2022) 121269

Contents lists available at ScienceDirect

Applied Catalysis B: Environmental

journal homepage: www.elsevier.com/locate/apcatb

Unraveling the active sites of Cs-promoted Ru/γ-Al_2O_3 catalysts for ammonia synthesis

Shih-Yuan Chen [a,*], Chih-Li Chang [b,1], Masayasu Nishi [a], Wei-Chih Hsiao [c,1], Yves Ira A. Reyes [d,1], Hiroyuki Tateno [a], Ho-Hsiu Chou [b,*], Chia-Min Yang [c,e,**], Hsin-Yi Tiffany Chen [d,*], Takehisa Mochizuki [a], Hideyuki Takagi [a,f], Tetsuya Nanba [g]

[a] Energy Catalyst Technology Group, Energy Process Research Institute (EPRI), National Institute of Advanced Industrial Science and Technology (AIST), 16-1 Onogawa, Tsukuba, Ibaraki 305-8559, Japan
[b] Department of Chemical Engineering, National Tsing Hua University, Hsinchu 300044, Taiwan
[c] Department of Chemistry, National Tsing Hua University, Hsinchu 300044, Taiwan
[d] Department of Engineering and System Science, National Tsing Hua University, Hsinchu 300044, Taiwan
[e] Frontier Research Center on Fundamental and Applied Sciences of Matters, National Tsing Hua University, Hsinchu 300044, Taiwan
[f] Global Zero Emission Research Center (GZR), National Institute of Advanced Industrial Science and Technology (AIST), 16-1 Onogawa, Tsukuba, Ibaraki 305-8559, Japan
[g] National Institute of Advanced Industrial Science and Technology (AIST), 16-1 Onogawa, Tsukuba, Ibaraki 305-8559, Japan

ARTICLE INFO

Keywords:
Ru catalyst
Dynamic Cs species
Active sites
Ammonia synthesis
Intermittent operation

ABSTRACT

The development of efficient and stable Ru catalysts is crucial for synthesis of decarbonized NH_3. Herein, a series of γ-Al_2O_3-supported Cs-promoted Ru catalysts were prepared, among which a 1.5Cs-Ru/γ-Al_2O_3 catalyst with a Cs/Ru molar ratio of 1.5 and a Ru size of ~2 nm exhibited high NH_3 synthesis rates (6.9–30 mmol g_{cat}^{-1} h^{-1}) at ~400 °C and 1 MPa. We unraveled that the surface acidity/basicity could be changed, and new active sites could be generated at the interfaces between the Ru particles and the CsOH-Cs^0 species by tuning the Cs/Ru molar ratio. Among the active sites, Cs^0 (minor), which transferred electrons to Ru, was present at the boundaries of the Ru particles and CsOH (major), which attracted the dissociative hydrogen atoms from the metallic Ru surfaces via a spillover effect and changed the surface acidity/basicity. This facilitated the adsorption/desorption of reactant species, thus promoting NH_3 synthesis.

1. Introduction

The world is heading into a new era of low-carbon sustainability through the use of hydrogen as a clean energy source—which results in low emissions of greenhouse gases and hazardous particulate matter—instead of burning fossil fuels [1,2]. NH_3 with a high hydrogen content (17.6%), which is produced using a well-developed industrial production chain and infrastructure, is a potential hydrogen carrier in a future hydrogen economy, and it will play a crucial role in ensuring that hydrogen production, transportation, and storage are safe [3]. However, industrial NH_3 synthesis relies on an Fe-catalyzed Haber–Bosch (HB) process that employs fossil-based energy and gray hydrogen and entails severe conditions (400–600 °C, 20–40 MPa). This process consumes approximately 1–2% of global fossil energy and consequently releases a large amount of CO_2, a key greenhouse gas that induces global warming and climate events [4–6]. To save energy and reduce CO_2 emissions, the KBR advanced ammonia process (KAAP) was commercialized in the 1990 s for the efficient, cost-effective synthesis of NH_3 over C-supported Ru catalysts, particularly Cs- and Ba-promoted versions, under relatively mild conditions [7–10]. It has been recently reported that these promoted Ru/C catalysts with increased porosity were efficient in low-pressure NH_3 synthesis under intermittent operation conditions, with green hydrogen obtained as a feedstock via the electrolysis of water using intermittent renewable electricity [11–14]. However, these

* Corresponding authors.
** Corresponding author at: Department of Chemistry, National Tsing Hua University, Hsinchu 300044, Taiwan.
E-mail addresses: sy-chen@aist.go.jp (S.-Y. Chen), hhchou@mx.nthu.edu.tw (H.-H. Chou), cmyang@mx.nthu.edu.tw (C.-M. Yang), hsinyi.tiffany.chen@gapp.nthu.edu.tw (H.-Y.T. Chen).
[1] These authors contributed equally to this work.

https://doi.org/10.1016/j.apcatb.2022.121269
Received 23 November 2021; Received in revised form 15 February 2022; Accepted 28 February 2022
Available online 10 March 2022

promoted Ru/C catalysts are deactivated via the sintering of Ru and the methanation of the C framework via hydrogen spillover [11,12]. Therefore, the development of highly efficient Ru catalysts with favorable textural properties and high stabilities for NH_3 synthesis remains necessary.

Al_2O_3 with a porous, rigid framework is a commonly used support in industrial catalysis [15]. For example, γ-Al_2O_3-supported MoS_2 catalysts with Co or Ni promotion are highly active in the hydrodesulfurization of crude oil, producing low-S fuels [16–20]. However, for Ru-catalyzed NH_3 synthesis, Al_2O_3-supported catalysts are less active than those supported on other inorganic oxides or carbons, owing to the high electronegativity of Al_2O_3, particularly γ-Al_2O_3. The addition of alkali or alkaline metals as promoters may improve the activities of Al_2O_3--supported Ru catalysts [7,21–26]. Among these, Cs is a commonly used promoter to improve the supported Ru catalysts for NH_3 synthesis [7]. However, the chemical states and structures of Cs and Ru active sites in NH_3 synthesis remain unclear. This is because the distribution of active components and their interactions can be significantly influenced by the type of metal precursor, the surface composition of the supporting material, and the method of catalyst preparation (Table 1 and references therein). Moreover, the chemical states and structures of active sites change during reductive activation and under catalytic reaction conditions with a varying gas composition. The pioneering works of Murata and Aika revealed that a Ru/γ-Al_2O_3 catalyst prepared using $Ru_3(CO)_{12}$ (entry 2) was superior in NH_3 synthesis to an analog prepared using $RuCl_3$ (entry 1) [22], and its activity was enhanced by an order of magnitude by adding a large amount of Cs (Cs/Ru molar ratios of 3–10, entries 3, 4, and 5) [23]. Miyazaki et al. further demonstrated that a Ru/γ-Al_2O_3 catalyst prepared using Cl-free Ru nanoparticles was more active than that prepared using Cl-containing Ru precursors (entry 6), because the Cl^- remained on the Ru surfaces [24,25]. Recently, Aika indicated that Cs, particularly CsOH, was present in the Cs-promoted Ru/MgO and Ru/Al_2O_3 catalysts [7]. The promotion effect of CsOH was minor in a Cs-Ru/Al_2O_3 catalyst with an acidic nature, even with a large Cs/Ru molar ratio (>10). Larichev et al. also indicated that Cs bound strongly to Al_2O_3 to form cesium aluminate, resulting in almost no activity of the Ru-Cs/Al_2O_3 catalyst in NH_3 synthesis (entry 7) [26]. On the other hand, Aika reported that a mixture of Cs^0 and CsOH on the $CsNO_3$-Raney Ru catalysts was formed following the process of reductive activation [27–29]. Raróg-Pilecka et al. studied the process of NH_3 synthesis using Cs-promoted Ru/C catalysts and suggested that Cs^0 present in close proximity to the Ru and Cs-adsorbed carbon moieties helped generate the electronic promotion effect [9]. Kowalczyk et al. claimed that the enhanced activity of the Cs-Ru/C catalysts could be potentially attributed to the strong electron donation from partially reduced Cs_xO_y (x/y = 2.7–3.6) present on the surfaces of the Ru particles but not the mixture of Cs^0 and CsOH [30]. Therefore, it was inferred that the structures of the Cs-promoted Ru active sites associated with NH_3 synthesis depend on the types of catalysts used and the methods of preparation followed. A consensus on the mechanism of formation and the roles of the catalysts is yet to be reached.

A commercial catalyst containing 5 wt% Ru/γ-Al_2O_3 with small Ru particles of ~2 nm (denoted Ru/γ-Al_2O_3) exhibited a high rate of NH_3 synthesis (r_{NH3}) of 1.85 mmol NH_3 g^{-1} h^{-1} at 500 °C under atmospheric pressure (entry 8). This is consistent with the computational studies reported by Honkala et al. and Hellman et al. that predicted increased N_2 activation by the B5 sites enriched in the ~2 nm Ru particles [31,32]. The r_{NH3} of the resulting Cs-promoted Ru/γ-Al_2O_3 catalyst, with a Cs/Ru molar ratio of 1.65 in the solid-state, was significantly enhanced to 5.0 mmol NH_3 g^{-1} h^{-1} at 400 °C at atmospheric pressure (entry 9) and 17 mmol NH_3 g^{-1} h^{-1} at 410 °C at 1 MPa (entry 10). In addition, the r_{NH3} in the range of 6.7–31 mmol NH_3 g^{-1} h^{-1} at ~400 °C responded rapidly to the reaction pressure, space velocity (SV), and H_2/N_2 ratio (e.g., low-pressure and intermittent operation conditions). The performance of the Cs-promoted Ru/γ-Al_2O_3 catalyst is comparable to those of new Ru catalysts on advanced supports, such as high-temperature-annealed Al_2O_3 (θ-Al_2O_3, entries 11–12) [33], a novel $12CaO{\cdot}7Al_2O_3$ electride (entry 13) [34], and rare earth oxides of Pr_2O_3 (entry 14) [35] and CeO_2 (entry 15) [36]. Owing to their considerable potential in industrial NH_3 synthesis, their performances in mild NH_3 synthesis, particularly green NH_3 synthesis under low-pressure conditions, should be evaluated. More importantly, the chemical states and structures of the active sites and their interactions should be investigated. Herein, Cs-promoted Ru/γ-Al_2O_3 catalysts with various Cs/Ru molar ratios of 0.25–5 (denoted as *x*Cs-Ru/γ-Al_2O_3, where *x* is the Cs/Ru molar ratio) were prepared via impregnation and evaluated in NH_3 synthesis under low-pressure and intermittent operation conditions (0.1–1 MPa, 300–550 °C, 6000–40000 h^{-1}, and H_2/N_2 = 0.2–5), which simulated the conditions of sustainable green NH_3 synthesis [10–15,37–43]. We focused on the influence of the Cs/Ru molar ratio on the chemical states and structures of the Cs and Ru active sites in NH_3 synthesis over the prepared *x*Cs-Ru/γ-Al_2O_3 catalysts, which were thoroughly characterized, including

Table 1
Previous studies on NH_3 synthesis activities (r_{NH3}) and corresponding reaction temperatures (T_{react}) of unpromoted and promoted Ru/γ-Al_2O_3 catalysts.

Entry	Catalyst	Ru precursor	Ru (wt%)	Cs precursor	Cs (wt%)	Cs/Ru	T_{react} (°C)	r_{NH3} (mmol NH_3 g^{-1} h^{-1})	P (MPa)	Ref.
1	Ru/γ-Al_2O_3	$RuCl_3$	1.9	–	–	–	400	0.008 (0.032)[a]	0.1	[22]
2	Ru/γ-Al_2O_3	$Ru_3(CO)_{12}$	2.1	–	–	–	400	0.062	0.1	[22]
3	Ru/γ-Al_2O_3	$Ru_3(CO)_{12}$	2.0	–	–	–	315	0.013	0.1	[23]
4	Cs-Ru/γ-Al_2O_3	$Ru_3(CO)_{12}$	2.0	$CsNO_3$	7.9	3.0	315	0.029	0.1	[23]
5	Cs-Ru/γ-Al_2O_3	$Ru_3(CO)_{12}$	2.0	$CsNO_3$	26.6	10.1	315	0.214	0.1	[23]
6	Ru/γ-Al_2O_3	Ru nanoparticles	6.3	–	–	–	450	0.923	0.1	[24,25]
7	Cs-Ru/γ-Al_2O_3	$RuOHCl_3$	4.5	Cs_2CO_3	4.0	0.8	400	inactive	0.1	[26]
8	Ru/γ-Al_2O_3[b]	–	5.0	Cs_2CO_3	–	–	504[c]	1.85[c]	0.1[c]	This work
9	1.5Cs-Ru/γ-Al_2O_3[d]	–	3.84[e]	Cs_2CO_3	8.34[e]	1.65[e]	398[c]	5.03[c]	0.1[c]	This work
10	1.5Cs-Ru/γ-Al_2O_3[d]	–	3.84[e]	Cs_2CO_3	8.34[e]	1.65[e]	410[f]	17[f]	1[f]	This work
11	Ru-Ba/γ-Al_2O_3[g]	$RuNO(NO_3)_3$	5.0	–	–	–	400	2.245	1	[30)]
12	Ru-Ba/θ-Al_2O_3[f]	$RuNO(NO_3)_3$	5.0		–	–	400	7.217	1	[30]
13	Ru/$C_{12}A_7$:e^-	$Ru_3(CO)_{12}$	4.0	–	–	–	400	2.12	0.1	[31]
14	Ru/Pr_2O_3	$Ru_3(CO)_{12}$	5.0	–	–	–	400	3.5	0.1	[32]
15	Ru/CeO_2	$RuC_{15}H_{21}O_6$	2.5	–			400	7~15	3	[33]

[a] The reduced sample was washed with 0.1% aqueous NH_3 solution.
[b] A commercial catalyst purchased from FUJIFILM Wako Pure Chemical (product code: 185–01042).
[c] Determined under ambient pressure conditions (space velocity (SV) = 3600 h^{-1}, H_2/N_2 molar ratio = 3) using the temperature-programmed surface reaction-mass spectrometry technique.
[d] The sample was prepared by impregnation of the material listed in Entry 8 with an aqueous Cs_2CO_3 solution.
[e] Determined using the inductively coupled plasma mass spectrometry (ICP-MS) technique.
[f] Performed under pressurized conditions (SV = 40,000 h–1, H_2/N_2 = 3).
[g] The Ba loading was 6 wt% based on Al_2O_3, corresponding to a Ba/Ru ratio of 1.8.

several in situ approaches for temperature-programmed reduction/desorption/surface reaction (TPR/TPD/TPSR) and X-ray absorption spectroscopy (XAS). These results were correlated with density functional theory (DFT) calculations, and the details of the active sites of NH_3 synthesis were elucidated.

2. Experimental section

2.1. Synthesis of Cs-Ru/γ-Al_2O_3

A commercial Ru/γ-Al_2O_3 catalyst was purchased from FUJIFILM Wako Pure Chemical (product code 185–01042, Osaka, Japan) and used as received. Cs_2CO_3 (99%, Alfa Aesar, Haverhill, MA, USA) was used as the Cs precursor as received. For Cs impregnation, 2.0 g Ru/γ-Al_2O_3 was dispersed in 50 mL of 1/1 v/v ethanol/water at ~20 °C, followed by the slow addition of 50 mL of Cs_2CO_3-containing ethanol/water (1/1 v/v, pH ~11), corresponding to Cs/Ru molar ratios of 0.25–5.0. The solvent was slowly evaporated at 80 °C and 0.05 bar, and the obtained powders were further dried at 100 °C overnight. The resulting samples are designated as-prepared xCs-Ru/γ-Al_2O_3, where x represents the nominal Cs/Ru molar ratio.

2.2. Characterization

Wide-angle X-ray diffraction (XRD) patterns were recorded in the 2θ range of 10–80 ° using a SmartLab SE instrument (Rigaku, Tokyo, Japan) operated at 40 kV and 30 mA, with Cu Kα radiation (λ = 1.5406 Å) used as the X-ray source. N_2 adsorption-desorption was measured using a Belsorp-Max instrument (Microtrac MRB, York, PA, USA) at 77 K. Prior to conducting the experiments, the samples were degassed at 150 °C for 6 h under high vacuum (~10^{-5} Pa). The specific surface area (S_{BET}) was calculated using the Brunauer−Emmett−Teller (BET) method in the P/P_0 range of 0.05–0.25. The total pore volume (V_{Total}) was determined till a P/P_0 ~0.95. The pore size distribution was obtained by analyzing the desorption isotherms using non-linear DFT (NLDFT). CO chemisorption was measured using a BELMETAL-3 instrument (Microtrac MRB) equipped with a thermal conductivity detector (TCD) at 50 °C using a stoichiometric CO/Ru value of 0.6 [10]. Prior to conducting the experiments, the samples were reduced at 350 °C using an H_2 gas flow of 50 mL min^{-1} for 2 h, followed by purging with He gas and cooling to 50 °C. For measurement, a sequential 5 vol% CO/He standard gas was pulsed over the reduced sample until no further CO adsorption was observed. All CO chemisorption data were measured at least three times, and the experimental errors of the corresponding Ru sizes were < ±0.1 nm. Field-emission scanning electron microscopy (FE-SEM) and energy-dispersive X-ray spectroscopy (EDS) techniques were used to analyze the samples. The experiments were performed using an SU8010 FE-SEM instrument (Hitachi, Tokyo, Japan) equipped with an EDS system (Horiba, Kyoto, Japan) and an S-4700 FE-SEM instrument (Hitachi) equipped with an EDS system (Horiba). High-resolution transmission electron microscopy (HR-TEM) was performed using a JEM-2100(HT) electron microscope (JEOL, Tokyo, Japan). Prior to observation, the samples were embedded in epoxy resin and cut into slices (~100 nm) using an Ultracut E ultramicrotome (Leica, Wetzlar, Germany). The size and size distributions of Ru were determined by counting ~100 particles in the HR-TEM images. XAS was conducted at the Ru *K*-edge and Cs L_3-edge using the transmission mode at beamlines TLS 01 C and TLS 17 C of the National Synchrotron Radiation Research Center (NSRRC, Hsinchu City, Taiwan) with a storage ring energy of 1.50 GeV and an electron beam current of 360 mA in top-up injection mode. The photon flux for the measurements was guided using a Si(111) monochromator, and the photon energy was calibrated using Ru (for Ru *K*-edge) or Ti (for Cs L_3-edge) foils. For the measurements, the catalyst was packed into an in situ cell with a Kapton window and reduced at 350 °C using an H_2 gas flow of 50 mL min^{-1} for 2 h. After the cell was cooled to approximately 20 °C, the X-ray absorption near-edge structure (XANES) and extended X-ray absorption fine structure (EXAFS) spectra were recorded. The average of multiple scans was used to improve the signal-to-noise ratio. Athena and Artemis programs (Demeter version 0.9.26) [44] were used for XAS data analysis.

2.3. Temperature-programmed studies

All G1-grade standard gases were purchased from TOMOE SHOKAI, Tokyo, Japan. Thermogravimetric analysis (TGA) and differential thermal analysis (DTA) were performed using a Thermo plus EVOA TG-DTA8122 instrument (Rigaku) at 30–1100 °C using 5 vol% H_2/Ar standard gas with a flow rate of 15 mL min^{-1}. Prior to H_2-TGA, the dried samples were placed in an Al_2O_3 pan and purged with N_2 gas (100 mL min^{-1}) for 30 min to eliminate oxygen. The TPR, TPD, and TPSR studies were performed using a BelCat II instrument (Microtrac MRB) equipped with a TCD and a BelMass mass spectrometer (Microtrac MRB). Prior to measurement, the dried samples (0.1–0.2 g) were packed into a quartz tube, sandwiched with quartz wood, and then assembled into the BelCat II instrument. The downstream from the catalyst bed was quantitatively analyzed by the mass spectrometry (MS) detector, which was calibrated using standard gases. All data were recorded at least three times, and their experimental errors were ~5–6%, potentially caused by weighing and the presence of adsorbed gases (adsorbed from the atmosphere). The H_2-TPR-MS profiles were recorded in the temperature range of 50–800 °C at a heating rate of 5 °C min^{-1} using 5 vol% H_2/Ar standard gas with a flow rate of 15 mL min^{-1}. The results were calibrated using 1 vol% H_2/Ar standard gas. For the TPSR studies, the dried samples were reduced using an H_2 gas flow (50 mL min^{-1}) at 350 °C for 2 h, followed by purging with Ar gas (50 mL min^{-1}) and cooling to 50 °C. After the TCD signal was stable for 1 h, the TPSR-MS data were recorded in the temperature range of 50–800 °C using a mixed gas flow of H_2 and N_2 (22.5 and 7.5 mL min^{-1}, respectively) passing over the reduced samples. The downstream H_2, N_2, and NH_3 concentrations were monitored using *m/z* ratios of 2, 28, and 16, respectively, and calibrated using a standard gas comprising 1 vol% H_2, 1 vol% N_2, and 1 vol% NH_3 balanced by Ar. The H_2-, N_2-, and NH_3-TPD-MS profiles were recorded. The data were recorded at 0–800 °C with a heating rate of 5 °C min^{-1} under Ar gas flow (15 mL min^{-1}) and calibrated using a standard gas comprising 1 vol% H_2, 1 vol% N_2, and 1 vol% NH_3 balanced by Ar. Prior to H_2- and N_2-TPD-MS measurement, the dried samples were reduced by H_2 gas flow (50 mL min^{-1}) at 350 °C for 2 h, followed by treatment with a mixed gas flow of H_2 and N_2 (30 mL min^{-1}, H_2/N_2 molar ratio = 0.2–5) at 400 °C and 0.1 MPa for 1 h. Prior to recording the NH_3-TPD-MS profiles, the dried samples were reduced at 350 °C under H_2 before the adsorption of NH_3, which served as a molecular probe at 0 °C. To avoid interference due to water (*m/z* ratios of 16–18), the NH signal, which was monitored using an *m/z* ratio of 15, was utilized to monitor NH_3. For CO_2-TPD-MS, the data were recorded at 0–800 °C at a heating rate of 5 °C min^{-1} under a flow of Ar gas (15 mL min^{-1}). The data were calibrated using a standard gas of 5 vol%CO_2/Ar. Prior to CO_2-TPD-MS, the samples were reduced at 350 °C under H_2 before the adsorption of CO_2, which served as a molecular probe at 50 °C.

2.4. Low-pressure NH_3 synthesis

NH_3 synthesis was performed in a fixed-bed stainless steel reactor under mild pressure (1 MPa). The downstream NH_3 concentration was quantitatively analyzed using an online gas chromatograph (GC) GC-2014 (Shimadzu, Kyoto, Japan) equipped with a TCD and a Thermon-3000 +KOH (2 + 2)% Sunpak-N 60/100 mesh column (2.1 m in length with an internal diameter of 3.2 mm, Shinwa Chemical Industries, Kyoto, Japan). All gas chromatography data were recorded five times after the steady-state conditions were maintained for > 30 min. The experimental error was < 7% (determined by analyzing three different runs conducted using the same catalyst). The as-prepared sample (~0.80 mL) was sandwiched in a quartz tube, followed by assembly

inside the fixed-bed stainless steel reactor. A thermocouple was inserted at the center of the catalyst bed to monitor the reaction temperature. The samples were progressively reduced by H_2 gas flow (100 mL min^{-1}) at 350 °C for 2 h prior to NH_3 synthesis. To commence NH_3 synthesis, the reactor was pressurized using a mixed gas flow of N_2 and H_2 (H_2/N_2 molar ratio = 3, SV = 9000 h^{-1}) up to ~1 MPa, which was controlled using a back-pressure regulator. The downstream NH_3 concentration was analyzed at a specific time in the temperature range of 300–600 °C. The SV and reaction pressure used in these conditions were much lower than those used during the conventional HB process because we aimed to study the process of small-scale NH_3 synthesis using low-carbon hydrogen under conditions of intermittent supply.

2.5. Computational Details

DFT calculations were performed using the Vienna *Ab initio* Simulation Package (VASP) [45–47]. Core electrons were treated with projector-augmented-wave (PAW) pseudopotentials [48,49]. Exchange and correlation interactions were treated using the Perdew-Burke-Ernzerhof (PBE) generalized gradient approximation (GGA) functional [50]. Cs-promoted Ru systems were modeled using Ru single atoms bonded to either Cs metal atoms or CsOH. The catalyst models were suspended in a vacuum inside a 15 Å × 15 Å × 15 Å box to minimize interactions with periodic images, and calculations were performed using a 405-eV plane-wave cutoff energy at the gamma point k-mesh until the change in energy between electronic loops was below 10^{-6} eV [51]. Geometries were optimized using the conjugate gradient algorithm until the forces upon each atom were < 0.01 eV $Å^{-1}$. The molecular and atomic adsorption of N_2 and H_2 on three Ru-based catalyst models, Ru, Ru-Cs, and Ru-CsOH, were examined. The adsorption energies per adsorbed atom (E_{ads}) were calculated as $E_{ads} = (E_{mol/Cat} - E_{Cat} - n * 0.5 * E_{mol})/n$, where $E_{mol/Cat}$ is the total energy of the complex, E_{cat} is the total energy of the bare Ru catalyst model, E_{mol} is the total energy of the H_2 or N_2 molecules, and n is the number of H or N atoms adsorbed. Generally, during DFT calculations, reversible adsorption and desorption of reactants are assumed. This was also the case assumed here. A lower or more negative E_{ads} implies stronger or more thermodynamically favorable adsorption and unfavorable desorption and vice versa. Atomic partial charges were calculated using Bader charge analysis [52,53].

3. Results and discussion

3.1. Low-pressure NH_3 synthesis (1 MPa)

Green NH_3 synthesis was recently demonstrated at Fukushima Renewable Energy Institute of AIST, Japan, using Ru-based catalysts at low pressure, where hydrogen with a low carbon footprint was synthesized using photovoltaic-based water electrolysis and used as a feedstock [37]. However, the performances of the unpromoted and promoted Ru-based catalysts were significantly influenced by the structures and kinetic behaviors of the active sites, which were related to reductive activation and reaction conditions, such as pressure, temperature, gas composition, flow rate, and other reaction parameters [11–15,38–43]. Herein, the performances of the Cs-Ru/γ-Al_2O_3 catalysts with various Cs/Ru molar ratios were studied under low-pressure NH_3 synthesis conditions to evaluate their potential industrial applications. Fig. 1A shows the temperature dependence of NH_3 production represented as vol% over the 0–5Cs-Ru/γ-Al_2O_3 catalysts under low-pressure conditions (1 MPa of H_2, an SV of 9000 h^{-1}, and an H_2/N_2 molar ratio of 3). For comparison, the r_{NH3} values are calculated by dividing the molar amount of formed NH_3 by the catalyst mass (Fig. S1A). Fig. 1**B** shows the maximum r_{NH3} and corresponding working temperature as a function of the Cs/Ru molar ratio. Because of the relatively low apparent activation energy (E_a) of 128 kJ mol^{-1} (Fig. S1B), 1.5Cs-Ru/γ-Al_2O_3 produces NH_3 at ~300 °C, with a maximum r_{NH3} of 9.7 mmol NH_3 g_{cat}^{-1} h^{-1} at 410 °C, which is much higher than those of other Cs-promoted Ru/γ-Al_2O_3 catalysts in the literature (Tables 1–2). The downstream NH_3 concentration is 2.5 vol% at 410 °C, which is slightly lower than the equilibrium value of 3.8 vol%. In contrast, the unpromoted Ru/γ-Al_2O_3 catalyst exhibits low activity at 410 °C, with a maximum r_{NH3} of 3.95 mmol NH_3 g_{cat}^{-1} h^{-1} observed at 500 °C, due to a relatively high E_a of 149 kJ mol^{-1}, potentially caused by the acidic nature of γ-Al_2O_3 [7,26,33]. A decrease in r_{NH3} and an increase in the corresponding reaction temperature are observed for the 0.5–1Cs-Ru/γ-Al_2O_3 catalysts, and the resulting values are between those corresponding to the Ru/γ-Al_2O_3 and 1.5Cs-Ru/γ-Al_2O_3 catalysts. Similar results are obtained when the Cs/Ru molar ratio is > 2. However, the decrease in the r_{NH3} of the 3–5Cs-Ru/γ-Al_2O_3 catalysts is relatively small when evaluated based on Ru loading in mmol g_{Ru}^{-1} h^{-1} (Fig. S2). Therefore, the influence of the Cs/Ru molar ratio on the performances of the prepared Cs-Ru/γ-Al_2O_3 catalysts in low-pressure NH_3 synthesis is higher than that of Ru loading. In addition, the Ru and Cs species formed at the active sites are likely suitable for improving a commercial 5 wt% Ru/γ-Al_2O_3 catalyst for low-pressure NH_3 synthesis when the Cs/Ru ratio is ~1.5–2. However, the E_a values of the 0.5–5Cs-Ru/γ-Al_2O_3 catalysts do not vary significantly with the Cs/Ru molar ratio, similar to the results of previous studies regarding mesoporous C-supported, Cs-promoted Ru catalysts in NH_3 synthesis [12].

The influence of the H_2/N_2 molar ratio (0.2–5) on the r_{NH3} of the 1.5Cs-Ru/γ-Al_2O_3 catalyst was studied at 1 MPa and an SV of 9000 h^{-1} using a mixed gas flow with various H_2/N_2 ratios. Fig. 2A and S3A show

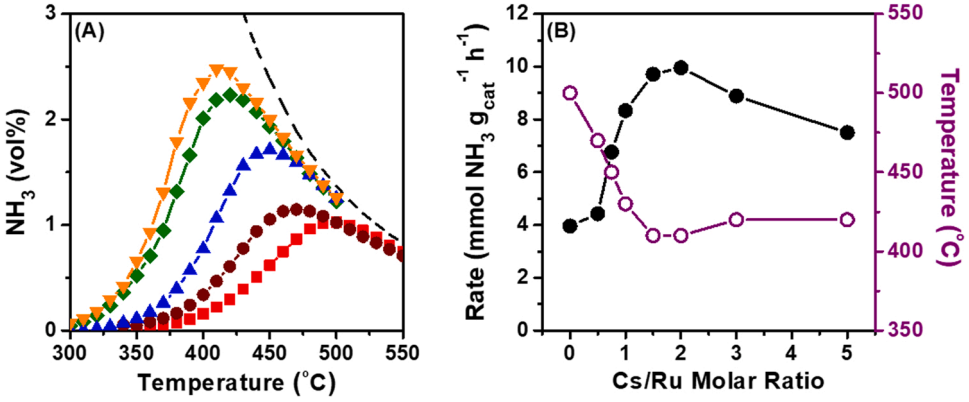

Fig. 1. (A) Temperature dependence of NH_3 synthesis over the prepared catalysts: (■) Ru/γ-Al_2O_3, (●) 0.5Cs-Ru/γ-Al_2O_3, (▲) 0.75Cs-Ru/γ-Al_2O_3, (◆) 1.5Cs-Ru/γ-Al_2O_3 and (▼) 5Cs Cs-Ru/γ-Al_2O_3 at 1 MPa and 9000 h^{-1} (H_2/N_2 = 3, mol/mol), using 1 g of catalyst (0.8 mL). **(B)** NH_3 synthetic activity and corresponding temperature as functions of the Cs/Ru molar ratio obtained at the maxima of the curves shown in Fig. S1(A).

Table 2
Structural properties and NH_3 synthetic activities of the as-prepared Cs-Ru/γ-Al_2O_3 catalysts.

Catalyst	Cs/Ru[a] (molar ratio)	S_{BET} (m^2 g^{-1})	V_{Total} (cm^3 g^{-1})	φ (nm)	Ru size (nm)		NH_3 synthesis		
					CO Chem.[b]	HR-TEM	NH_3 synthetic activity (mmol NH_3 g^{-1} h^{-1})[c]	Temp. (°C)[c]	Activation energy (kJ mol^{-1})[d]
Ru/γ-Al_2O_3	–	107	0.27	5.4	2.2	2.2	3.95	500	149
0.75Cs-Ru/γ-Al_2O_3	0.74	96	0.22	5.8	1.9	2.0	6.76	450	132
1.5Cs-Ru/γ-Al_2O_3	1.65	78	0.21	5.6	2.1	2.3	8.50	410	128
5Cs-Ru/γ-Al_2O_3	5.73	33	0.13	5.8	3.2	2.4	6.33	420	125

[a] Determined using the ICP-MS technique.
[b] Determined using CO pulse chemisorption at least five times. The experimental errors are ± 0.1 nm.
[c] Measured at 1 MPa and 9000 h^{-1} ($H_2/N_2 = 3$).
[d] Calculated using an Arrhenius plot (Fig. S1). HR-TEM, high-resolution transmission electron microscopy. φ, pore diameter.

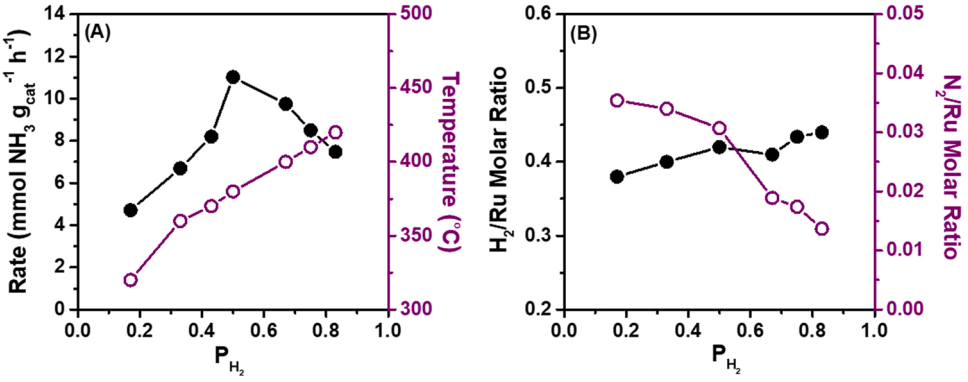

Fig. 2. (A) Effect of H_2/N_2 molar ratio on the maximum NH_3 synthetic activity and corresponding temperature over 1.5Cs-Ru/γ-Al_2O_3 at 1 MPa and 9000 h^{-1} using a mixed gas flow with H_2 partial pressures in the range of 0.17–0.83 (Fig. S2) and (B) N_2- and H_2-temperature-programmed desorption-mass spectrometry study of the 1.5Cs-Ru/γ-Al_2O_3 catalysts after treatment with various H_2/N_2 flows (Fig. S4).

that the r_{NH3} of the 1.5Cs-Ru/γ-Al_2O_3 catalyst exhibits a volcano relationship with the H_2/N_2 molar ratio. A maximum r_{NH3} of 12 mmol NH_3 g_{cat}^{-1} h^{-1} is observed at an H_2/N_2 molar ratio of 1 at a corresponding working temperature of 380 °C. This is different from the Fe-catalyzed HB process, which is optimized at an H_2/N_2 molar ratio of 3. This result is similar to that of our recent study of low-pressure NH_3 synthesis over the Cs-promoted Ru/@SBA-15 catalyst, which exhibits a maximum r_{NH3} at an H_2/N_2 molar ratio of 1 due to hydrogen poisoning [15]. Brown et al. indicated that the H_2/N_2 molar ratio is optimized at 2.2 in the commercial KAAP using a Ru-based catalyst due to the different kinetic characteristics of Ru and Fe catalysts [8]. TPD-MS was utilized to study the surface H_2 and N_2 residues on the used 1.5Cs-Ru/γ-Al_2O_3 catalysts, which were treated with various feedstocks (characterized by H_2/N_2 molar ratios in the range of 0.2–5) at 400 °C and 0.1 MPa for 1 h, corresponding to the H_2 partial pressures in the range of 0.16–0.83. Fig. 2B and S3B show that the N_2/Ru molar ratios on the used 1.5Cs-Ru/γ-Al_2O_3 catalysts decrease when the H_2 partial pressures in the feedstocks are increased. The H_2/Ru molar ratios differ by one order of magnitude and increase linearly when the H_2 partial pressure is increased to 0.5. The values remain nearly unchanged at higher H_2 partial pressures. The desorption temperatures corresponding to surface H_2 and N_2 residues are slightly influenced by the feedstock H_2 partial pressure (Fig. S4). Therefore, the active sites of the 1.5Cs-Ru/γ-Al_2O_3 catalyst are more accessible to the N_2 molecules at relatively low feedstock H_2 partial

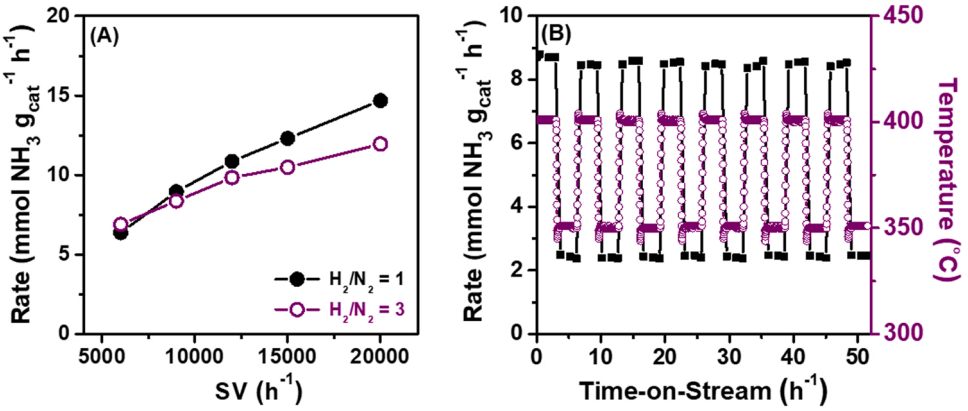

Fig. 3. Intermittent NH_3 synthesis over 1.5Cs-Ru/γ-Al_2O_3 at reaction conditions of (A) 1 MPa and 6000–20 000 h^{-1} using mixed H_2 and N_2 gases at an H_2/N_2 molar ratio of 1 or 3 and (B) 1 MPa and 350–400 °C with an SV of 9000 h^{-1} using mixed H_2 and N_2 gases at an H_2/N_2 ratio of 3.

pressures.

Intermittent NH_3 synthesis over 1.5Cs-Ru/γ-Al_2O_3 was examined by varying the SV and H_2/N_2 molar ratios at 1 MPa and 400 °C (Fig. 3A and **S5A**). When the SV is increased from 6000 to 20000 h^{-1} and the H_2/N_2 molar ratio is maintained at 1, a progressive increase in r_{NH3} over 1.5Cs-Ru/γ-Al_2O_3 is observed. When the H_2/N_2 molar ratio is increased to 3, the increase in r_{NH3} over 1.5Cs-Ru/γ-Al_2O_3 is hindered as the SV increases, potentially due to hydrogen poisoning. A similar trend is observed when the SV is further increased in the range of 20000–40000 h^{-1} (Figure S6), which is similar to the conditions of the industrial HB process. Although high-pressure reactions should be studied more, it can be said that 1.5Cs-Ru/γ-Al_2O_3 is a potential candidate for small-scale synthesis of green NH_3 and large-scale conventional HB processes with improved energy efficiencies, such as the KAAP. A rapid change in the reaction temperature at 350 and 400 °C was further studied over eight cycles, corresponding to a reaction time of ~50 h. This simulated a portable, small-scale NH_3 synthesis plant with rapid startup properties. The SV and H_2/N_2 molar ratios were maintained at 9000 h^{-1} and 3, respectively. Fig. 3B shows that the r_{NH3} of 1.5Cs-Ru/γ-Al_2O_3 is rapidly tuned between 2.46 and 2.49 mmol NH_3 g_{cat}^{-1} h^{-1} at 350 °C and between 8.37 and 8.70 mmol NH_3 g_{cat}^{-1} h^{-1} at 400 °C. The catalytic performance remains almost unchanged after eight cycles (>50 h). Thus, 1.5Cs-Ru/γ-Al_2O_3, characterized by high activity, good stability, and rapid responsivity, exhibits the potential to catalyze low-pressure, intermittent NH_3 synthesis reactions.

3.2. Characterization

To understand the structures and chemical states of the active sites in NH_3 synthesis and their interactions, the prepared Cs-Ru/γ-Al_2O_3 catalysts were systematically characterized using *ex situ* and in situ techniques. The results are divided into two parts: (i) characterization of the bulk catalysts and (ii) activation in relation to the formation of active sites. In part (i), the physicochemical properties of the as-prepared samples were studied using conventional characterizations, including XRD, N_2 physisorption, CO chemisorption, ICP-MS, X-ray fluorescence (XRF), high-resolution SEM-EDS, and HRTEM. Characterization was extended to the reduced/passivated samples, and the used samples were studied after pressurized NH_3 synthesis (Fig. 1A). In part (ii), reductive activation to produce the Cs-Ru active sites for NH_3 synthesis was studied using temperature-programmed methods (including H_2-TGA, H_2-TPR-MS, and TPD-MS) and in situ XAS in relation to the data obtained from part (i) and DFT calculations. During activation, the as-prepared samples were reduced at 350 °C for 2 h using an H_2 gas flow of 50 mL min^{-1}, which was the same as the reductions in Section 3.1 and part (i). We particularly focused on the influence of the Cs/Ru molar ratio on the structures and chemical states of the Cs-promoted Ru active sites, which are activated for NH_3 synthesis after reductive activation. The reactive species of H_2 and N_2 (likely from feedstock and NH_x) remaining on the Cs-promoted Ru active sites during ambient-pressure NH_3 synthesis were also studied using TPD-MS and correlated to the Cs-promoted Ru active sites indicated by characterization. The results of Ru/γ-Al_2O_3, 0.75Cs-Ru/γ-Al_2O_3, 1.5Cs-Ru/γ-Al_2O_3, and 5Cs-Ru/γ-Al_2O_3 are described below. Further detailed data are presented in the ESI.

3.3. Characterization of bulk catalysts

The XRD patterns reveal diffraction peaks at 2θ = 20°, 32°, 37°, 39°, 46°, 60°, and 67° corresponding to the (111), (220), (331), (222), (440), (511), and (400) planes of γ-Al_2O_3, respectively, and their intensities decreased with increasing Cs/Ru ratio (Figure 4A) [54,55]. The N_2 physisorption isotherms indicate that the mesoporous structure of γ-Al_2O_3 is affected by Cs impregnation, appearing to collapse at a high Cs/Ru ratio of 5 (Figure 4**B** and Table 2 and **S1**). Thus, the crystalline framework of γ-Al_2O_3 is affected by the impregnation of basic Cs solutions (pH = 11.0–12.5). The diffraction peaks of RuO_2 at 2θ = 28.3° and 35.2°, representing the (110) and (101) planes, respectively, are very small [56]. Cs is not observed using XRD, with the exception of the new diffraction peaks at 2θ = 26–27° for 5Cs-Ru/γ-Al_2O_3, similar to those observed for the Cs_2CO_3 precursor (Figure S7). Small RuO_2 particles (<5 nm) may be present in the as-prepared 0.5–5Cs-Ru/γ-Al_2O_3 with amorphous or semi-crystalline Cs_2CO_3-like species [11,12].

The XRD patterns and N_2 adsorption-desorption isotherms of the reduced/passivated and used catalysts are similar to those of the as-prepared catalysts (Fig. S8–9). The peaks representing RuO_2 are hardly observed using XRD, and thus they cannot be used to estimate the RuO_2 particle sizes using the Scherrer equation. Table 2 shows that the S_{BET} values, V_{Total} values, and pore diameters of the as-prepared Cs-Ru/γ-Al_2O_3 catalysts gradually decrease with increasing Cs/Ru molar ratios, particularly for 3–5Cs-Ru/γ-Al_2O_3, where the mesoporous structure is collapsed by the strongly basic Cs solution. However, the structural properties of the as-prepared samples are similar to those of the reduced/passivated and used samples, indicating that the reduction/passivation and reaction conditions exert no significant influence on the

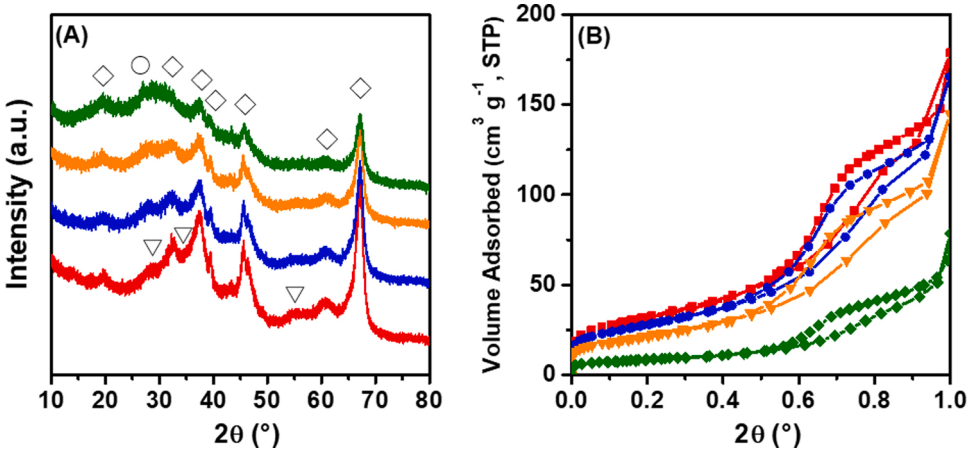

Figure 4. (A) X-ray diffraction patterns and (B) N_2 adsorption–desorption isotherms of the as-prepared catalysts: (—, ■) Ru/γ-Al_2O_3, (—, ●) 0.75Cs-Ru/γ-Al_2O_3, (—, ▲) 1.5Cs-Ru/γ-Al_2O_3, and (—, ▼) 5Cs-Ru/γ-Al_2O_3. The labels ⋄, ▽, and ○ represent γ-Al_2O_3, RuO_2, and Cs_2CO_3, respectively.

structural properties of the bulk (Fig. 5A).

ICP-MS and XRF show that the Cs/Ru ratios of the as-prepared, reduced/passivated, and used Cs-Ru/γ-Al_2O_3 catalysts are similar to the nominal values used in the preparations (Table 2 and S1–3). The size of Ru was analyzed using CO chemisorption. The results reveal that the Ru sizes corresponding to Ru/γ-Al_2O_3 and 0.5–2Cs-Ru/γ-Al_2O_3 are approximately 2 nm, varying slightly with the Cs/Ru molar ratio. In contrast, 3–5Cs-Ru/γ-Al_2O_3 exhibit relatively large Ru particles (2.6–3.2 nm), which are positively correlated to the Cs/Ru molar ratio. The influence of the Cs/Ru molar ratio on the morphology and Ru size/size distribution of the as-prepared Cs-Ru/γ-Al_2O_3 was then investigated using FE-SEM-EDS and ultramicrotome HR-TEM. As shown in Figs. S10–13, the FE-SEM-EDS images reveal that all samples are irregular aggregates with homogeneously dispersed Ru and Cs species, with the exception of needle-like aggregates present in 5Cs-Ru/γ-Al_2O_3. The needle-like aggregates are associated with Cs_2CO_3 crystallites due to excess Cs impregnated in 5Cs-Ru/γ-Al_2O_3. The FE-SEM-EDS images of the reduced/passivated and used catalysts are similar to those of the as-prepared samples, indicating that Cs and Ru are stable after reductive activation and NH_3 synthesis. The ultramicrotome HR-TEM images show that dark dots representing 2–2.4-nm RuO_2 particles are present in the as-prepared samples (Fig. S14) regardless of the Cs/Ru molar ratio. The results are similar to those obtained using CO chemisorption, with the exception of those of 3–5Cs-Ru/γ-Al_2O_3 with 14–29 wt% Cs (Fig. 5B). Therefore, CO chemisorption on the Ru particle surfaces is influenced by the Cs species, exaggerating the Ru particle size.

3.4. Reductive activation in relation to active site formation

The Cs-promoted Ru catalysts are generally activated at 300–500 °C using H_2 gas flow or a mixed H_2/N_2 gas prior to NH_3 synthesis [57–67]. This is reductive activation, which was studied using H_2-TGA and H_2-TPR-MS (Figs. 6 and 7). The results are compared with those of commercial RuO_2 (FUJIFILM Wako Pure Chemical) and Cs_2CO_3 (Alfa Aesar) products (Fig. S15). 1.5Cs_2CO_3/RuO_2 was prepared by impregnating RuO_2 with Cs_2CO_3 (64.7 wt%) of RuO_2, corresponding to a Cs/Ru molar ratio of 1.5, which corresponds to the Cs/Ru molar ratio of 1.5Cs-Ru/γ-Al_2O_3. 1.5Cs_2CO_3/γ-Al_2O_3 was prepared by impregnating γ-Al_2O_3 with Cs_2CO_3 (10.8 wt%), which is equal to the Cs loading of 1.5Cs-Ru/γ-Al_2O_3. In the H_2-TGA thermogram of RuO_2, a distinct mass loss of 23.9% is observed at 140–185 °C, with the DTA signal centered at 165 °C (Fig. S15A), corresponding to RuO_2 reduction to Ru metal. This is consistent with the calculated value of 24.1% (Eq. 1).

$$RuO_{2(s)} + 2H_2 \rightarrow Ru_{(s)} + 2H_2O_{(g)},\ -24{\cdot}1\% \quad (1)$$

The TGA thermogram of Cs_2CO_3 exhibits a mass loss of 0.8% at < 80 °C, which is related to the removal of adsorbed H_2O species, a mass loss of 4.7% at 80–180 °C, which is related to the removal of adsorbed CO_2 species, and a complete mass loss at > 680 °C, with two endothermal peaks centered at 790 and 920 °C. This complete mass loss is associated with the phase transition and decomposition of Cs_2CO_3 (melting point = 610 °C) to the corresponding molten salts, such as Cs_2O (melting point = 490 °C) and CsOH (melting point = 272 °C; boiling point = 990 °C), and simultaneous gasification (Eq. 2 and Fig. S15B). For comparison, the TGA of $Cs_2CO_{3(s)}$ was also conducted in air. $Cs_2CO_{3(s)}$ decomposition and subsequent gasification are observed at relatively high temperatures, with two endothermal peaks centered at 795 and 1000 °C (Fig. S16). Hence, Cs_2CO_3 is thermally stable up to ~680 °C in a reductive atmosphere and ~750 °C in air.

$$Cs_2CO_{3(s)} \rightarrow Cs_2O_{(g)} + CO_{2(g)} \quad (2)$$

For 1.5Cs/RuO_2, two mass losses of 21.8% and 8.9% are observed at 150–220 °C (centered at 195 °C) and 620–760 °C (centered at 700 °C), respectively (Fig. S15C). The 21.8% mass loss is related to RuO_2 reduction, which is slightly hindered in the presence of Cs species. However, it is much larger than the calculated value (–8.5%, Eq. 3) because more H_2O and CO_2 may be adsorbed on 1.5Cs/RuO_2. In addition, the hydrogenolysis of Cs_2CO_3, which produces CsOH and CO, may occur in this temperature range due to the presence of hydrogen with Cs and Ru species (Eq. 4). The other mass loss (8.9%) is slightly lower than the calculated value (9.6%) for $Cs_2CO_{3(s)}$ decomposition to the corresponding molten salts (Eq. 5a) and much lower than the calculated value of 31% (Eq. 5b) for $Cs_2CO_{3(s)}$ decomposition and subsequent gasification. This observation is slightly different from that reported previously by Aika et al., indicating that $CsNO_3$ decomposed to CsO_2 during the reduction of the $CsNO_3$-Raney Ru mixture [27–29]. CsO_2 may further decompose to CsOH and Cs, which gets immediately evaporated as the melting point is low [28]. As Cs species do not spill from the H_2-TGA analysis, and the mass loss is close to that presented in Eq. (4), it is speculated that caesium oxides, such as Cs_2O and CsOH molten salts, may interact with the Ru metals derived during the reduction of 1.5Cs/RuO_2, hindering gasification.

$$RuO_{2(s)} + 2\ H_{2(g)} + 0{\cdot}75Cs_2CO_{3(s)} \rightarrow Ru_{(s)} + 2\ H_2O_{(g)} + 0{\cdot}75Cs_2CO_{3(s)},\ -8{\cdot}5\ wt\% \quad (3)$$

$$Ru_{(s)} + 0{\cdot}75Cs_2CO_{3(s)} + 0{\cdot}75\ H_{2(g)} \rightarrow Ru_{(s)} + 1{\cdot}5CsOH_{(l)} + 0{\cdot}75CO_{(g)},\ -5{\cdot}6\ wt\%\ (hydrogenolysis) \quad (4)$$

$$Ru_{(s)} + 0{\cdot}75Cs_2CO_{3(s)} \rightarrow Ru_{(s)} + 0{\cdot}75Cs_2O_{(l)} + 0{\cdot}75CO_{2(g)},\ -9{\cdot}6\ wt\%\ (decomposition) \quad (5a)$$

$$Ru_{(s)} + 0{\cdot}75Cs_2CO_{3(s)} \rightarrow Ru_{(s)} + 0{\cdot}75Cs_2O_{(g)} + 0.75CO_{2(g)},\ -31\ wt\%\ (decomposition) \quad (5b)$$

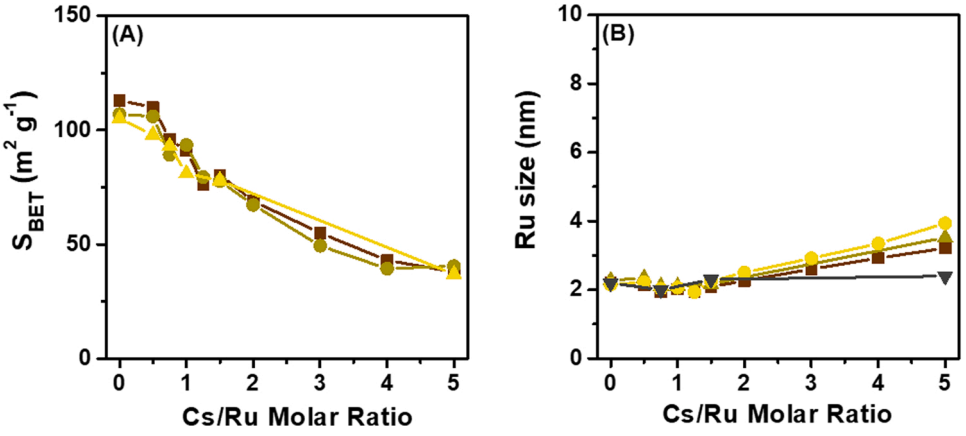

Fig. 5. Effect of Cs/Ru molar ratio on the (A) specific surface area (S_{BET}) and (B) Ru sizes of the (■) as-prepared, (●) reduced/passivated, and (▲) used catalysts. The symbol (▼) in B represents the Ru sizes estimated using the high-resolution transmission electron microscopy technique.

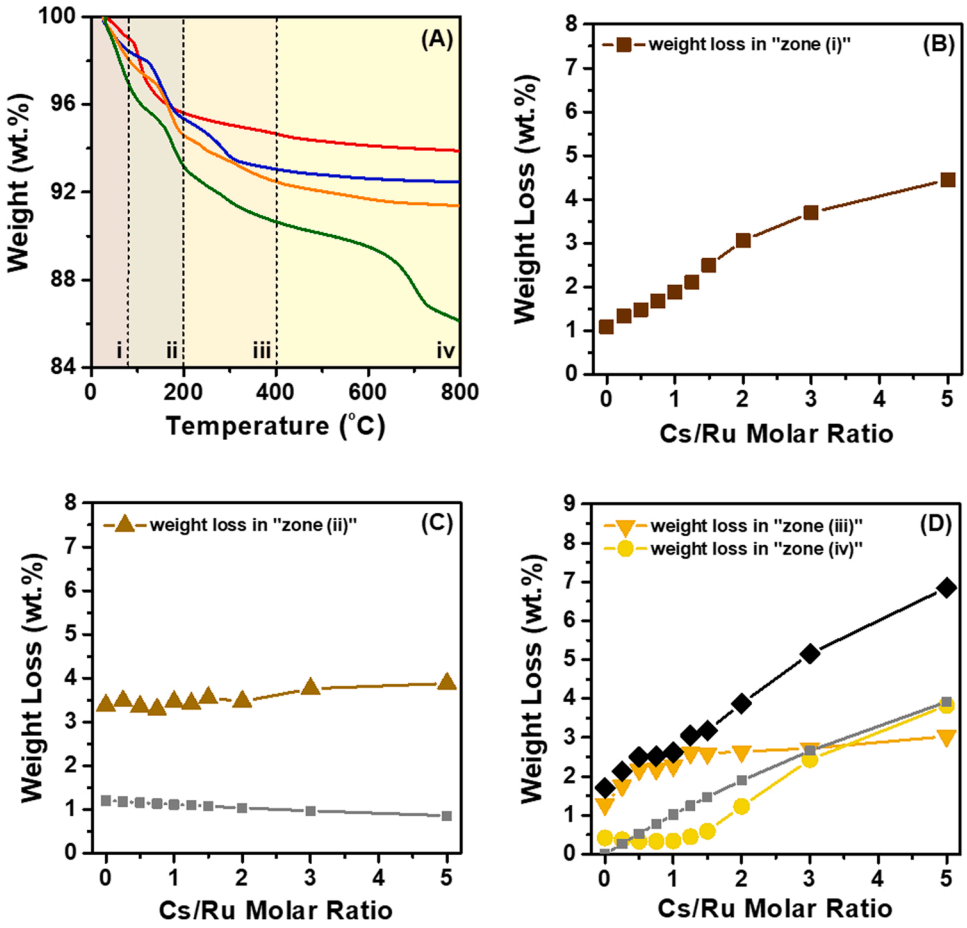

Fig. 6. (A) H_2-thermogravimetric analysis thermograms of (—) 5 wt% Ru/γ-Al_2O_3, (—) 0.75Cs-5 wt% Ru/γ-Al_2O_3, (—) 1.5Cs-5 wt% Ru/γ-Al_2O_3, and (▼) 5Cs-5 wt% Ru/γ-Al_2O_3, obtained using a standard gas of 5% H_2/Ar with a flow rate of 15 mL min^{-1} and a heating rate of 5 °C min^{-1}, and the dependence of the mass losses on the Cs/Ru molar ratio in the temperature ranges of (B) zone (i), (C) zone (ii), which is related to RuO_2 reduction, and (D) zones (iii) and (iv), which are related to the hydrogenolysis and thermal decomposition of Cs_2CO_3. The symbols (▼) and (●) represent the mass losses in zones (iii) and (iv), respectively. The symbol (◆) represents the sum of the mass losses in zones (iii) and (iv). The gray curves (gray square, ■) in Fig. 6C and D show the calculated mass losses of the conversions of RuO_2 to Ru and Cs_2CO_3 to CsOH.

For 1.5Cs/γ-Al_2O_3, a gradual 7.8% mass loss is observed at < 200 °C (Figure S15D), which is 1.4 times higher than that of Cs_2CO_3, as more H_2O and CO_2 species may be adsorbed on the Cs species-impregnated γ-Al_2O_3. The other mass loss is 0.65% at > 600 °C, associated with Cs_2CO_3 decomposition and further condensation of γ-Al_2O_3. This mass loss is lower than the calculated value for $Cs_2CO_{3(s)}$ decomposition to caesium oxides (e.g., 1.5% using Eq. 6). Cs_2CO_3 strongly interacts with γ-Al_2O_3 at a Cs_2CO_3 loading of 10.8 wt%, with its decomposition and gasification hindered even at a high temperature and under a reduced atmosphere.

$$10{\cdot}8\ \text{wt\%}\ Cs_2CO_{3(s)}/\gamma\text{-}Al_2O_{3(s)} \rightarrow 9{\cdot}3\ \text{wt\%}\ Cs_2O_{(l)}/\gamma\text{-}Al_2O_{3(s)} + yCO_{2(g)},\ -1{\cdot}5\ \text{wt\%}. \quad (6)$$

Three distinct mass losses are observed for the commercial Ru/γ-Al_2O_3 catalyst (Fig. 6). At < 80 °C, the 1.1% mass loss is associated with H_2O desorption. At 80–200 °C, the other 3.4% mass loss is related to RuO_2 reduction to Ru. However, it is higher than the calculated value (1.3%), as the CO_2 species (2.1%) derived from the atmosphere are adsorbed on Ru/γ-Al_2O_3 and potentially desorb at 80–200 °C. Another mass loss of 1.7% is observed at 200–800 °C due to further Al_2O_3 condensation. The H_2-TGA thermograms of the as-prepared Cs-Ru/γ-Al_2O_3 catalysts are divided into four temperature zones: (i) H_2O desorption at < 80 °C, (ii) RuO_2 reduction to Ru at 80–200 °C [27–29], (iii) hydrogenolysis of relatively small Cs_2CO_3 at 200–500 °C, which is likely facilitated by the metallic Ru particles, and (iv) decomposition of relatively large Cs_2CO_3, forming CsOH, at 500–800 °C (Fig. 6 A and S17). Fig. 6B–D show the dependence of the mass losses in temperature zones (i–iv) on the Cs/Ru molar ratios of the as-prepared Cs-Ru/γ-Al_2O_3 catalysts. The mass losses in zones (ii) and (iv) are higher than the calculated values due to CO_2 desorption and further condensation of γ-Al_2O_3, respectively (Fig. S18). For zone (i), increasing mass loss is observed with increasing Cs/Ru molar ratios, indicating that the amount of H_2O adsorbed on the Cs-Ru/γ-Al_2O_3 catalysts is increased by the impregnation of the hydrophilic, basic Cs_2CO_3 species (Fig. 6B). For zone (ii), a slight increase in mass loss is observed upon increasing the Cs/Ru molar ratio, particularly for high Cs/Ru ratios of 2–5 (Fig. 6 C and S18B). These mass losses are 2–3 wt% higher than the calculated values for RuO_2 → Ru because atmospheric CO_2 species are adsorbed on the Cs-Ru/γ-Al_2O_3 catalysts. For zone (iii), the mass loss increases linearly when the Cs/Ru molar ratio is increased to 0.5 and increases slightly at higher Cs/Ru molar ratios. This mass loss is associated with the hydrogenolysis of relatively small Cs_2CO_3 species, which should be close to the interface of the metallic Ru particles and γ-Al_2O_3, and is likely due to hydrogen spillover from the metallic Ru particles [27–29,68]. However, the reverse is true for the mass loss in the zone (iv), which is associated with the decomposition of relatively large Cs_2CO_3 species. This is only observed when the Cs/Ru molar ratio is > 1.5, suggesting that relatively large Cs_2CO_3 species are formed in the 1.5–5Cs-Ru/γ-Al_2O_3 catalysts.

To better understand the Cs-Ru active sites formed during reductive activation, H_2-TPR-MS was performed (Fig. 7 and S19) using the same procedure as that used for H_2-TGA. The hydrogen consumption was

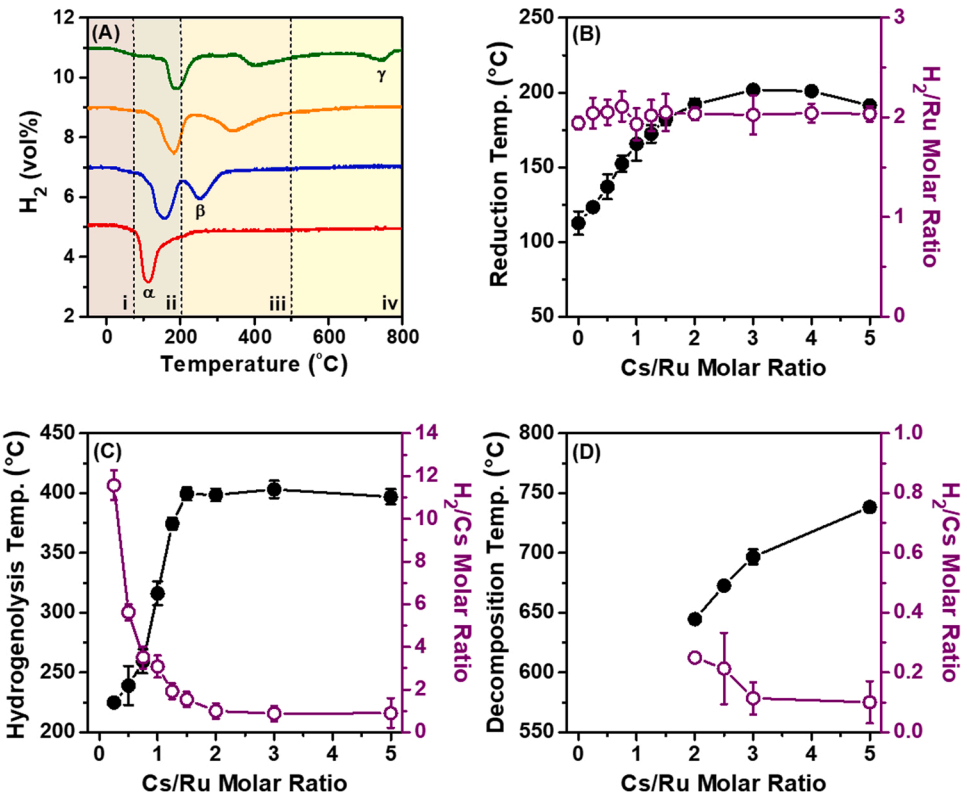

Fig. 7. (A) H_2-temperature-programmed reduction-mass spectrometry profiles of the as-prepared catalysts: (—) Ru/γ-Al_2O_3, (—) 0.75Cs-Ru/γ-Al_2O_3 shifted in 2 vol%, (—) 1.5Cs-Ru/γ-Al_2O_3 shifted in 4 vol%, and (▼) 5Cs-Ru/γ-Al_2O_3 shifted in 6 vol%. (B) Reduction temperature and corresponding H_2/Ru molar ratio as functions of Cs/Ru molar ratio, (C) hydrogenolysis temperature and corresponding H_2/Cs molar ratio as functions of Cs/Ru molar ratio, and **(D)** decomposition temperature and corresponding H_2/Cs molar ratio as functions of Cs/Ru molar ratio.

quantitatively calculated using a 1 vol% H_2/Ar standard gas. All data were measured three times, and the standard deviations are shown in Fig. 7B–D. The H_2-TPR-MS profiles of the as-prepared Cs-Ru/γ-Al_2O_3 catalysts are compared with those of RuO_2 (Figure S20), Cs_2CO_3 (Figure S21), 1.5Cs/RuO_2 (Fig. S22), and 1.5Cs/γ-Al_2O_3 (Fig. S23). For RuO_2, a one-step reduction to Ru is observed at 160 °C, accompanied by the release of H_2O, and the H_2/Ru molar ratio is ~2. CH_4, CO, and CO_2 are also detectable because CO_2 desorbs from RuO_2 and is partially hydrogenated to CO and CH_4. For Cs_2CO_3, the removal of adsorbed CO_2 species is observed at 200 °C, while its decomposition is observed at temperatures > 600 °C, accompanied by the release of CO and CO_2. 1.5Cs/RuO_2 shows a one-step reduction of RuO_2 to Ru, with an H_2/Ru molar ratio of ~2 at 184 °C (Fig. S22), which is hindered by the Cs species. Meanwhile, CO_2 desorbs and is partially hydrogenated to CO and CH_4, similar to that desorbed from RuO_2 (Fig. S20). At temperatures > 400 °C, CO and CO_2 are observed due to the hydrogenolysis and decomposition of Cs_2CO_3, respectively, with the partial reduction of CO_2 to CH_4 catalyzed by the Ru metal. A large amount of CO_2, along with CO and H_2O, desorbs from 1.5Cs/γ-Al_2O_3 at < 500 °C (Figure S23). Cs_2CO_3 decomposition is almost negligible, indicating that Cs strongly interacts with γ-Al_2O_3 at a Cs loading of 10.8 wt%. These results are consistent with the results obtained using the H_2-TGA technique.

The H_2-TPR-MS profiles of the as-prepared Cs-Ru/γ-Al_2O_3 catalysts show three distinct signals: (a) RuO_2 reduction, centered at 120–200 °C (signal α), corresponding to zone (ii) in the H_2-TGA thermograms; (b) hydrogenolysis of relatively small Cs_2CO_3 species, centered at 225–400 °C (signals β), corresponding to zone (iii) in the H_2-TGA thermograms; and (c) the decomposition of relatively large Cs_2CO_3 species at temperatures > 500 °C (signal γ), corresponding to zone (iv) in the H_2-TGA thermograms. The hydrogen consumption is represented as the H_2/Ru molar ratio (Fig. 7) or H_2/Cs molar ratio (Fig. 7C–D), which are correlated with the Cs/Ru molar ratio and proposed reactions (Eqs. 1–6).

As shown in Fig. 7B, the reduction temperature of the α signal increases linearly from 120° to 180°C with increasing Cs/Ru molar ratio up to 1.5–2 and varies slightly with a further increase in the Cs/Ru molar ratio. This result is similar to that of 1.5Cs/RuO_2 and our recent study regarding Cs-Ru/@SBA-15 catalysts for NH_3 synthesis, which showed that RuO_2 reduction was slightly hindered by the presence of Cs [13]. However, the H_2/Ru molar ratios are ~2, indicating that RuO_2 may be completely reduced at ~200 °C. The results agreed with the results reported previously, indicating that the unpromoted and Cs-promoted Ru/Al_2O_3 catalysts could be completely reduced at ~150 °C, although the extent of hydrogen consumption realized was higher than equivalent [27]. As shown in Fig. 7(C), the hydrogenolysis temperature of the β signal also increases with an increase in the Cs/Ru molar ratio to 1.5–2 and remains almost unchanged at higher Cs/Ru molar ratios. However, the reverse is true for the H_2/Cs molar ratio (>1.5), which is inconsistent with Eq. (4). As shown in Fig. S19, large amounts of CH_4 accompanied by small amounts of H_2O and CO are observed when the Cs/Ru molar ratios are < 1. In contrast, an increase in CO and decreases in H_2O and CH_4 are observed at higher Cs/Ru molar ratios. Karm et al. demonstrated that the migration of hydrogen (i.e., hydrogen spillover) from Al_2O_3-supported Pt particles to neighboring iron oxide particles and the subsequent reduction is limited to 15 nm. Cs_2CO_3 may be finely dispersed on the Cs-Ru/γ-Al_2O_3 catalysts with relatively low Cs/Ru molar ratios (<1.5). When the finely dispersed Cs_2CO_3 species are close to the metallic Ru particles, they are easily converted to CsOH and CO via hydrogenolysis. Similar results were reported previously when the reduction behavior of caesium hydroxide-added Ru-based catalysts and $CsNO_3$-Raney Ru catalyst was studied by Aika et al [27,28]. CO may be simultaneously reduced by the spillover hydrogen, yielding CH_4 with the release of H_2O. Further, CO_2, which is likely mostly derived from the atmosphere, is also observed in zones (i–iii) at an order of magnitude lower than that of CO. Regarding the higher Cs/Ru molar ratios, Cs_2CO_3

is fully impregnated on 1.5–2Cs-Ru/γ-Al_2O_3 and further aggregates into semi-crystallites on 3–5Cs-Ru/γ-Al_2O_3. The hydrogenolysis of Cs_2CO_3 to CsOH and subsequent CO hydrogenation only occurs at the interfaces of the metallic Ru particles (Eq. 4). The remaining Cs_2CO_3 may undergo decomposition (Eq. 5a). As shown in Fig. 7D, from the γ signals, the temperatures corresponding to the decomposition of relatively large Cs_2CO_3 to Cs_2O are observed for 3–5Cs-Ru/γ-Al_2O_3 and the H_2/Cs molar ratios are significantly small (<0.3). This is consistent with the H_2-TGA thermograms and the above theory.

XAS was used to analyze and compare the oxidation states of Ru and Cs in the Cs-Ru/γ-Al_2O_3 catalysts before and after reductive activation. Fig. 8 shows the XANES spectra at the Ru *K*-edge. The spectra of all samples before reductive activation resemble that of bulk RuO_2, with absorption edges at 22129.8 eV (Fig. 8A), indicating that the Ru oxidation states are 4^+ in all as-prepared samples regardless of the Cs/Ru molar ratio. After reductive activation, the absorption edges of all Cs-Ru/γ-Al_2O_3 catalysts shift to lower energies almost identical to that of metallic Ru (22117.0 eV) (Fig. 8B). The Fourier transform profiles of the k^3-weighted EXAFS spectra of the reductively activated catalysts and Ru foil are shown in Figure S24. The fitted results (Table S4) indicate that the Ru species in all Cs-Ru/γ-Al_2O_3 catalysts are mostly reduced to metallic Ru nanoparticles, with coordination numbers smaller than that of the metallic Ru foil [69]. However, in situ XAS and H_2-TPR-MS techniques could only be used to obtain the average chemical states of the Ru species in the as-prepared and reduced samples. Distinct boundaries are not observed for the Ru particles and alumina. The hydrogen consumption behavior determined using the H_2-TPR-MS technique may be affected by the sample mass and the type of adsorbed species present in the atmosphere and during the experiments. Qin et al. recently reported that the alkali ions might suppress the reduction and aggregation of Ru over alumina-supported Ru catalysts [70]. Therefore, we speculated that the Ru species were mostly reduced to metallic Ru nanoparticles (exception: the boundaries of Ru and alumina).

XAS at the Cs L_3-edge (corresponding to the $2p_{3/2} \rightarrow 6$ s/5d transition) was conducted, and the XANES spectra of each catalyst before and after reductive activation are compared (Fig. 9A–B and S25). Because of the detection limit, we were unable to acquire the Cs L_3-edge XANES spectra of the samples with Cs/Ru molar ratios of < 0.75. The white-line intensity of the Cs L_3-edge is associated with the average oxidation state of the metal: the lower the average oxidation state, the lower the white-line intensity due to the lower transition probability to the half-occupied 6 s orbital of Cs^0 as compared to that to the empty 6 s orbital of Cs^{1+} [71,72]. Decreases in the white-line intensities are observed after reductive activation for all Cs-Ru/γ-Al_2O_3 catalysts, with the exception of that with a Cs/Ru molar ratio of 5. As shown in Fig. 9C, the differences in the white-line intensities of the catalysts before and after reductive activation (ΔI_{WL}) are plotted as a function of the Cs/Ru molar ratio. The catalyst with a Cs/Ru molar ratio of 0.75 exhibits the largest ΔI_{WL}, which decreases with increasing Cs/Ru molar ratio. Therefore, the Cs^{1+} species (i.e., those formed via hydrogenolysis of Cs_2CO_3 to CsOH) in the Cs-Ru/γ-Al_2O_3 catalysts are partially reduced to Cs^0 as the dynamic species that are only formed and present during reductive activation and even under working conditions. In addition, because the fraction of Cs reduced in the catalysts should correlate positively with the ΔI_{WL}, the amount of Cs^0 formed may be similar for all Cs-Ru/γ-Al_2O_3 catalysts. Analysis of the H_2-TPR-MS profiles reveals that Cs reduction during the process of reductive activation is likely not directly associated with H_2. It can potentially be influenced by the spillover hydrogen species that are cleaved from the metallic Ru nanoparticles [27–29,68]. This hypothesis is similar to that put forward in a recent paper by Eslava et al. They reported that the partial reduction of Cs occurred in the region proximal to the Cs (derived from CsCl) and small Ru particles (~1 nm, derived from $RuCl_3 \cdot xH_2O$) on high-surface-area graphite during reductive activation (400 °C in 10 vol%H_2/He). They also reported that the reduced Cs species might allow the electron enrichment of Ru for CO activation for Fischer–Tropsch reaction [72]. However, the amount used to fabricate the catalyst and roles of the reduced Cs species in the Cs-promoted Ru/γ-Al_2O_3 catalysts may be different from the amounts used to fabricate the Ru-Cs/C catalyst and the roles in the Ru-Cs/C catalyst as the properties of γ-Al_2O_3 and C are different.

Scheme 1 illustrates the proposed active sites of the Cs-Ru/γ-Al_2O_3 catalysts for NH_3 synthesis, which vary according to the Cs/Ru molar ratio. The inferences are based on experimental results (particularly those obtained using the XRD, H_2-TGA, H_2-TPR-MS techniques), in situ XAS results, and previously proposed models [7,27,29]. Ru is mostly formed as Ru metal (exception: RuO_x at the boundaries of the Ru particles and γ-Al_2O_3) [70]. Cs is first held on the acidic sites of γ-Al_2O_3, stuck to Ru boundaries (particularly those characterized by the Cs/Ru molar ratios in the range of 1–2), and aggregated to semi-crystalline Cs_2CO_3 at higher Cs/Ru molar ratios. Fig. 10 shows the performances and surface Cs densities of the various Cs-Ru/γ-Al_2O_3 catalysts. At low Cs/Ru molar ratios (<1.5) and surface Cs densities (<3 atom nm^{-2}), Cs_2CO_3 is finely impregnated on the Cs-Ru/γ-Al_2O_3 catalysts and may be hydrogenolyzed to CsOH during reductive activation, particularly on the neighboring metallic Ru particles [27–29]. This generates CO, which may be simultaneously reduced to CH_4 by spillover hydrogen from the metallic Ru particles. Meanwhile, CsOH is partially reduced to metallic Cs species (yellow part of Scheme 1) at the boundaries of the Ru particles and CsOH. This can be attributed to the hydrogen spillover phenomenon (from the Al_2O_3-supported Ru particles to the neighboring Cs species) [27–29,68]. The CsOH and Ru species, with reduced Cs species at the interfaces, are proposed as the CsOH-Cs^0/Ru active sites for NH_3 synthesis. When the Cs/Ru molar ratios are in the range of 1.5–2 and the surface Cs densities are in the range of 3–7 atom nm^{-2}, the CsOH-Cs^0/Ru

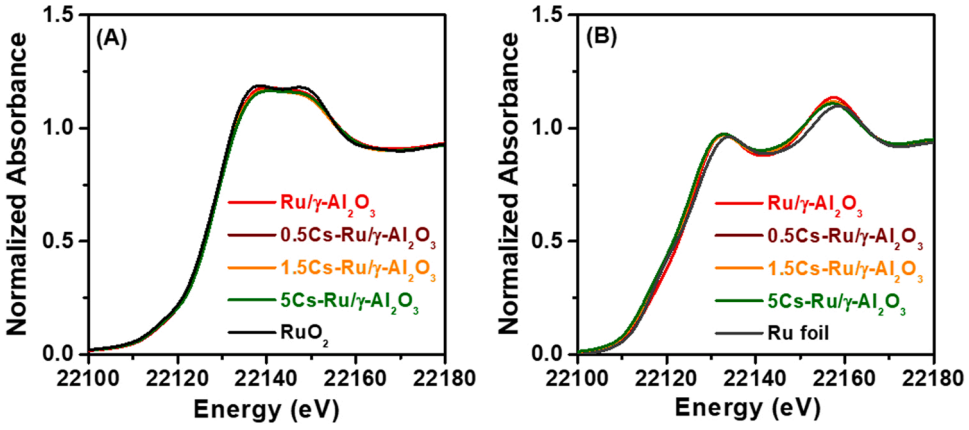

Fig. 8. *In situ* Ru *K*-edge X-ray absorption near-edge structure spectra of the (A) as-prepared catalysts in air (compared with the profiles recorded for RuO_2), and (B) H_2-reduced catalysts (compared with the profiles recorded for the Ru foil).

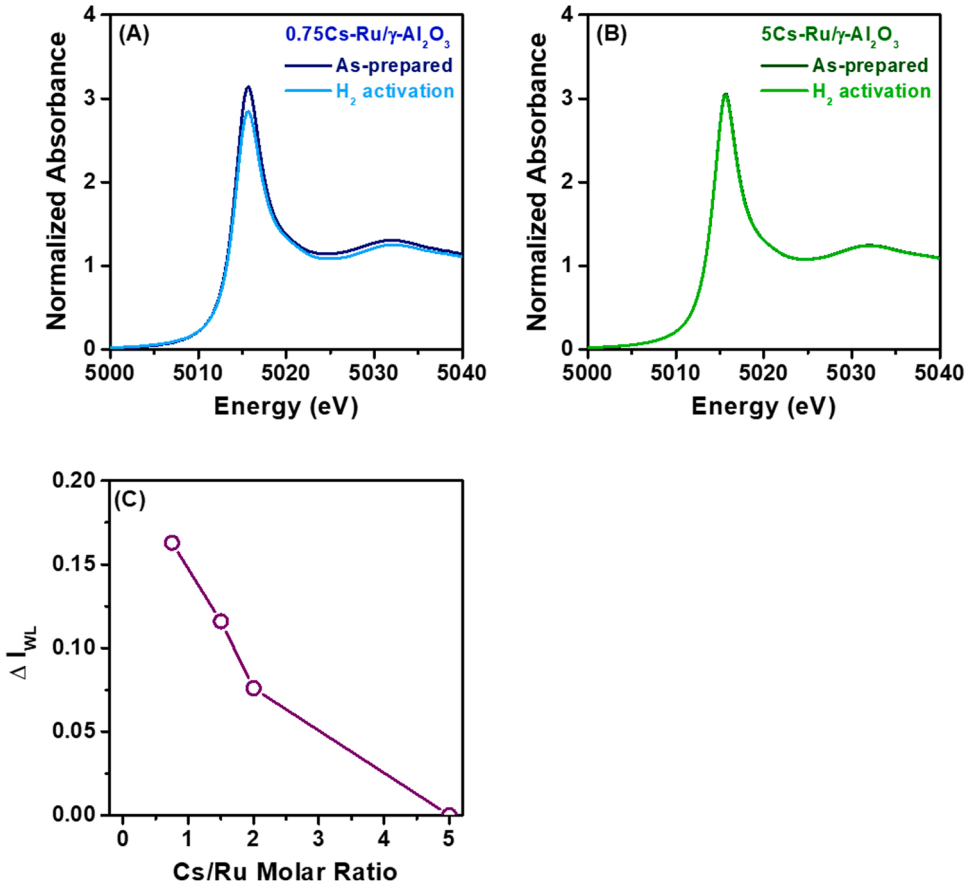

Fig. 9. (A,B) *In situ* Cs L_3-edge X-ray absorption near-edge structure spectra of 0.75Cs-Ru/γ-Al_2O_3 (A) and 5Cs-Ru/γ-Al_2O_3 (B) before (as-prepared) and after H_2 activation. (C) Plot of the differences in the white-line intensity before and after H_2 activation (I_{WL}) as a function of the Cs/Ru molar ratio.

active sites are maximized, exhibiting high activity during NH_3 synthesis. It is worth mentioning that these CsOH-Cs^0/Ru active sites, particularly metallic Ru and reduce Cs species, in the Cs-promoted Ru/γ-Al_2O_3 catalysts are produced following the process of reductive activation and during the synthesis of ammonia. At high Cs/Ru molar ratios of 2–5 and surface Cs densities of 7–28 atom nm^{-2}, the excess Cs_2CO_3 gradually aggregates into semi-crystallites, which are stable under working conditions and exhibit no significant influence on NH_3 synthesis.

DFT calculations were performed to understand the influences of the two types of promoters, Cs and CsOH, on the adsorption/desorption behaviors of H_2 and N_2 on the Ru-based catalysts in terms of adsorption energies, structures, and charge distributions. To exclude the Ru cluster size, morphology, and metal-support interaction effects, we employed single Ru atom models. Hence, as shown in Fig. 11, three models were constructed to represent the Ru-based catalyst: (i) a Ru single atom (denoted Ru), (ii) a Ru atom bound to Cs (denoted as Ru–Cs), and (iii) a Ru atom bound to CsOH (denoted Ru–CsOH). The results of Bader charge analysis indicate that Ru gains (−0.69 |e|) electrons from Cs^0 in the Ru–Cs model, which is more than the (−0.20 |e|) electrons gained from CsOH in the Ru–CsOH model. Therefore, Cs is a stronger electronic promoter than CsOH. H_2 and N_2 adsorption on the Ru, Ru–Cs, and Ru–CsOH models were then analyzed. It reveals the barrier-less dissociative adsorption of H_2 to 2 H, with adsorption energies of − 0.65, − 0.85, and − 0.83 eV and final H–H distances (d_{H-H}) of 1.88, 2.34, and 1.82 Å on Ru, Ru–Cs, and Ru–CsOH, respectively, compared to the calculated initial d_{H-H} of 0.75 Å of an H_2 molecule in the gas phase. In contrast, N_2 is molecularly adsorbed, with two possible configurations: (a) monodentate, representing N_2 adsorption perpendicular to the catalytic surface, or (b) bidentate, representing N_2 adsorption parallel to the catalytic surface. The adsorption energies are − 0.72, − 1.07, and − 0.97 eV for (a) and − 0.39, − 0.98, and − 0.55 eV for (b) on Ru, Ru–Cs, and Ru–CsOH, respectively. The DFT calculations indicate that monodentate N_2 * (d_{N-N} = 1.15, 1.17, and 1.19 Å on Ru, Ru–Cs, and Ru–CsOH, respectively) is the more stable configuration compared to the more activated bidentate N_2 * (d_{N-N} = 1.19, 1.20, and 1.21 Å on Ru, Ru–Cs, and Ru–CsOH, respectively), which is associated with the intermediates of the surface dissociation of N_2 * to 2 N * . These results are consistent with previous DFT analyses using Ru slab models, indicating that the Ru, Ru–Cs, and Ru–CsOH models are reliable models that can be used for understanding the active sites associated with ammonia synthesis [73,74].

The barrier-less dissociative adsorption of H_2 to 2 H* may lead to high H* coverage on the Ru surface and thus hinder N_2 * adsorption on the Ru surface because of the occupation of adsorption sites. This leads to the experimentally observed H poisoning of Ru [75,76] and Ru/γ-Al_2O_3 catalysts (this study). The presence of Cs species, Cs^0 or CsOH, improves the adsorption of the reactants, particularly that of the bidentate N_2 * , which may facilitate N_2 * adsorption and compete with H adsorption on the promoted Ru. This indicates the potential to reduce the extent of H poisoning realized. With respect to charge transfer and distribution (Fig. 11), the changes in the Bader charge of Ru are approximately zero |e| and from − 0.4 to − 0.5 |e| for Ru–CsOH and Ru–Cs, respectively, compared to those of Ru in the unpromoted Ru–2 H, Ru–N_2 (monodentate), and Ru–N_2 (bidentate). This confirms that CsOH is not as effective as Cs as an electron donor. In addition, for N_2 adsorption on Ru–CsOH, the Bader charge values of N and Cs are approximately − 0.10 to − 0.39 |e| and 0.8 |e|, respectively, with N–Cs distances of ~4.7 Å (Table S5). In comparison, the N and Cs Bader charges of Ru–Cs are approximately − 0.13 to − 0.45 |e| and 0.7 |e|,

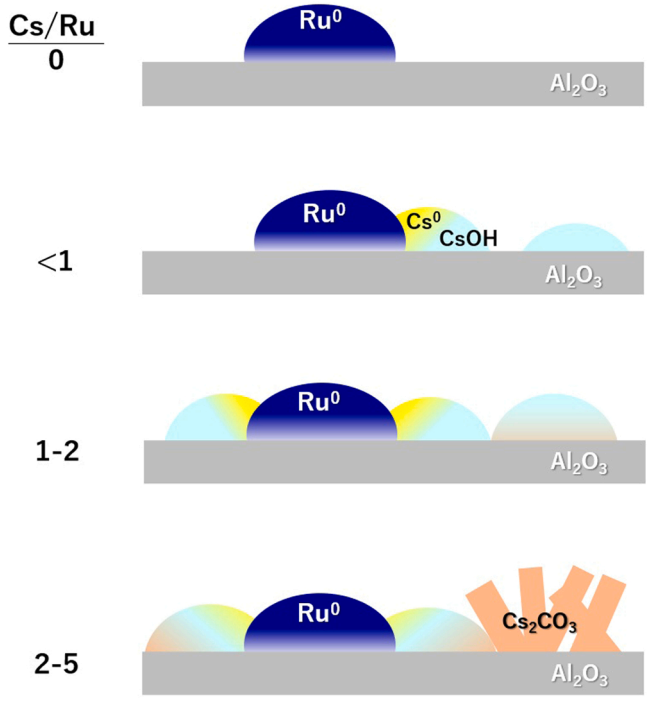

Scheme 1. Proposed Cs-Ru active sites of the Cs-Ru/γ-Al_2O_3 catalysts under working conditions of NH_3 synthesis, where the Ru particles (blue) are supported on γ-Al_2O_3 (gray) with boundaries of RuO_x (pale blue). Cs^0 (yellow) is formed at the boundaries of the Ru particles and CsOH (bright blue), which is held by the acidic sites of γ-Al_2O_3. These stick to the Ru boundaries as the Cs/Ru molar ratio is increased. Cs_2CO_3 (pale brown) is formed under conditions of high Cs/Ru molar ratios (>1.5). (For interpretation of the references to colour in this figure, the reader is referred to the web version of this article.)

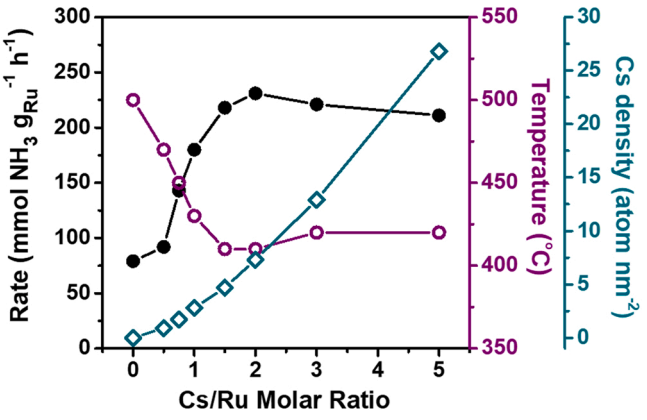

Fig. 10. Correlation of Cs/Ru molar ratio and Cs density with the rate of NH_3 synthesis and corresponding working temperature over the Cs-Ru/γ-Al_2O_3 catalysts. The catalytic data were obtained from Fig. S2).

respectively, with Cs–N distances of ~3 Å. Thus, the direct electrostatic attraction between the promoter and adsorbed N_2 is less pronounced in Ru–CsOH than that in Ru–Cs. The latter is consistent with published results [74]. However, the former is different from the results of previous studies, which claimed that CsOH is an electron promoter that modifies the electronic environment of Ru for N_2 activation [7,75,76]. With regard to H_2 adsorption, we intentionally positioned H_2 away from the Ru–CsOH and Ru–Cs interfaces. After optimization, H_2 spontaneously chemisorbs at the Ru–Cs bridge sites of Ru–CsOH and Ru–Cs (Fig. S26 animation), indicating that CsOH and Cs promoters may offer new active sites. Similarly, N_2 may be stabilized on both active sites,

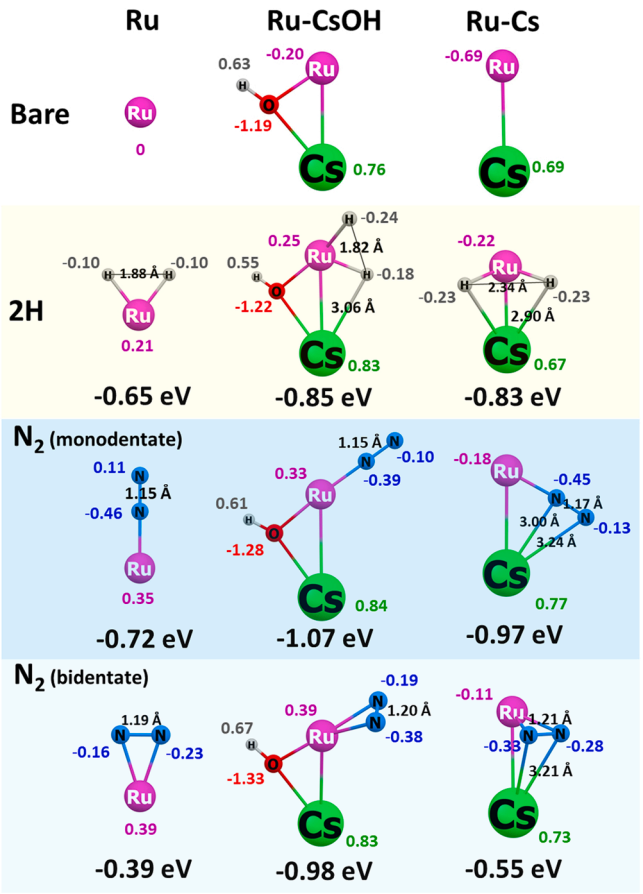

Fig. 11. Ru, Ru–Cs, and Ru–CsOH model catalysts (*from top to bottom*) in their bare form, with 2 H* atoms adsorbed, and with an N_2 * molecule adsorbed in a mono- or bidentate configuration. The corresponding adsorption energies per atom for the 2 H* and N_2* structures are displayed in black below each structure. The pink, green, red, gray, and blue spheres represent Ru, Cs, O, H, and N atoms, respectively (these structures are all optimized using density functional theory). The calculated Bader charge of each atom is indicated.

away from and in the vicinity of the Ru–promoter (CsOH and Cs) interfacial sites. In short, both Cs and CsOH promote NH_3 synthesis by offering adsorption sites for H* to minimize the H poisoning of the Ru sites, making them available for N_2 adsorption (i.e., both species offer new active sites). However, the electronic promoter effect of Cs is more pronounced.

To gain deep insight into the active sites associated with NH_3 synthesis, the surface basic and acidic properties of the unpromoted and Cs-promoted Ru/γ-Al_2O_3 catalysts were further analyzed using the NH_3- and CO_2-TPD-MS techniques, respectively (Figs. S27-S28 and Table S6). Analysis of the CO_2-TPD-MS profiles revealed that the surface basicities of the Cs-promoted Ru/γ-Al_2O_3 catalysts were higher than those of the unpromoted Ru/γ-Al_2O_3 catalyst and the surface basicity was positively correlated with the Cs/Ru molar ratio. The amounts of CO_2 desorption (indicated by peaks centered at ~110 °C and >420 °C) increased with increasing Cs/Ru molar ratios (exception: 5Cs-Ru/γ-Al_2O_3). The intensities of the CO_2 signals appearing at ~110 °C (for 5Cs-Ru/γ-Al_2O_3) were lower and the intensities of the peaks appearing at > 420 °C were higher than the peaks corresponding to Ru/γ-Al_2O_3 and 0.5–1.5Cs-Ru/γ-Al_2O_3. This suggests that CO_2 may get absorbed by 5Cs-Ru/γ-Al_2O_3 to form relatively large Cs_2CO_3 species, which get decomposed at > 420 °C. These data are consistent with the proposed active sites and surface structures of the Cs-promoted Ru/γ-Al_2O_3 catalysts fabricated by varying the Cs/Ru molar ratios (Scheme 1).

The NH_3-TPD-MS profiles were analyzed. It was observed that the

NH signals (corresponding to NH_3) associated with the unpromoted and Cs-promoted Ru/γ-Al_2O_3 catalysts were of significantly low intensity. Highly intense H_2 signals and weak N_2 signals were observed. The temperature regions corresponding to NH desorption (corresponding to NH_3) were different from those corresponding to H_2 and N_2. This suggested that the NH_3 species adsorbed on the reduced samples might decompose to form H_2 and N_2 during the NH_3-TPD-MS-based experiments, even at 0 °C. These species may get redistributed on the catalyst surface. The amounts of H_2 species remaining on the reduced samples decrease with increasing Cs/Ru molar ratio. The corresponding desorption temperature was low. N_2 can be readily purged from the reduced samples, such that the remaining amount of N_2 is an order of magnitude lower than the amount of H_2. Thus, the adsorption and desorption of H_2, N_2, and NH_3 are facilitated by the addition of Cs to the Ru/γ-Al_2O_3 catalysts. Lin et al. reported that the K-promoted Ru/C catalysts adsorbed more amounts of hydrogen than the unpromoted Ru/AC catalysts. They also reported that the adsorption strength for N_2 or NH_3 was weakened [77]. As observed for K-promoted Ru/AC catalysts, the addition of Cs to the Ru/γ-Al_2O_3 catalysts may influence the structures and adsorption/desorption properties of the active sites. The extent of influence exerted, in this case, was higher than the extent of influence exerted by the electronic promotion effect. The acidic nature of γ-Al_2O_3 should be further considered.

The reaction orders were kinetically analyzed to study the adsorbed species at the active sites associated with NH_3 synthesis in the presence of the Cs-promoted Ru/γ-Al_2O_3 catalysts (Table 3). These were studied using a mixed flow of H_2 and N_2 gases in the temperature range of 400–500 °C following the procedures reported previously [78]. These results are correlate with the amounts of surface hydrogen and nitrogen residues on the used catalysts obtained by analyzing the H_2- and N_2-TPD-MS profiles (Fig. 12 and S29), and the surface acidities/basicities obtained by analyzing the NH_3- and CO_2-TPD-MS profiles (Figs. S27–28). The reaction order (n) for N_2 is ~1, indicating that N_2 dissociation is the rate-determining step for the Ru/γ-Al_2O_3 and Cs-promoted Ru/γ-Al_2O_3 catalysts. This is consistent with our hypothesis that the electronic promotion effects of the Ru and CsOH active sites with reduced Cs species are small, corresponding to the relatively high E_a values (120–150 kJ mol^{-1}) for NH_3 synthesis. According to the results obtained using the in situ XAS analysis and the temperature-programmed study combined with DFT calculations, Cs^0 (minor) is only present at the boundaries of Ru and CsOH (major), and it contributes to N_2 dissociation. But this contribution would be limited due to a low amount of Cs^0. The reaction orders (a) and (h) for NH_3 and H_2 are –1.1 and 0.2, respectively, for the Ru/γ-Al_2O_3 catalyst. It reveals that the Ru/γ-Al_2O_3 catalyst is poisoned by NH_3 at 430 °C and not by H_2. This can be attributed to the acidic γ-Al_2O_3 surface. The result is consistent with the result reported previously by Aika et al. They indicated that NH_3 (or NH_x intermediates) is mostly adsorbed at the acidic sites of the Ru/γ-Al_2O_3 catalysts, and H_2 and N_2 are simultaneously adsorbed on the Cs-promoted Ru/γ-Al_2O_3 catalysts. When the catalyst mass was doubled at 430 °C and 1 MPa, the reaction order corresponding to the Ru/γ-Al_2O_3 catalyst remained almost unchanged. However, the (a) and (h) values increased to − 0.5 and 0.6, respectively, and the (n) value remained unchanged when the reaction temperature was increased to 500 °C at 1 MPa using 0.05 g of the catalyst. This indicated that the extent of poisoning of the NH_x species on the Ru/γ-Al_2O_3 catalyst could be reduced under conditions of high reaction temperatures. However, the NH_x species can potentially decompose to form H_2 and N_2. H_2 may remain on the surface of Ru, resulting in hydrogen poisoning. This hypothesis is supported by the results obtained using the H_2- and N_2-TPD technique, which revealed that H_2 largely remained on the Ru/γ-Al_2O_3 catalyst and was desorbed at a relatively high temperature centered at ~320 °C. In contrast, the amount of the N_2 residue was low, and this could be attributed to the rapid desorption. Hence, the Ru/γ-Al_2O_3 catalyst was poisoned by NH_3, which was potentially adsorbed on the acidic Al_2O_3-supported Ru surface. H_2 poisoning might be induced by the process of NH_3 decomposition.

For the 0.75–5Cs-Ru/γ-Al_2O_3 catalysts, the reaction orders (a) and (h) change to values ranging from approximately − 0.2 to − 0.3 and from − 0.3 to − 0.6, respectively. This could be attributed to the Ru and CsOH active sites containing reduced Cs species at their interfaces and the neutralization of the acidic sites by the Cs species (Scheme 1). The reaction order (h) of 1.5–5Cs-Ru/γ-Al_2O_3 is more positive than that of 0.75Cs-Ru/γ-Al_2O_3, whereas the variation in the reaction order (a) is negligible. The analysis of the H_2- and N_2-TPD profiles further reveal that the amount and desorption temperature of the H_2 residues are reduced by increasing the Cs loading amount (Table 3 and Fig. S29). Moreover, an increase in the amount of the N_2 residues is observed at a relatively low temperature. Results obtained by analyzing the NH_3-TPD-MS profiles revealed that NH_3 decomposed to form H_2 and N_2 over unpromoted and Cs-promoted γ-Al_2O_3 catalysts (Fig. S28). The amounts of the H_2 and N_2 residues on the Cs-promoted γ-Al_2O_3 catalysts were lower than the amounts recorded on the unpromoted γ-Al_2O_3 catalyst (Table S6). Therefore, it can be concluded that the addition of Cs to the Ru/γ-Al_2O_3 catalysts not only generates new active sites at the interfaces between the Ru particles and the Cs^0/CsOH species, but it also alters the surface basicities/acidities, facilitating the adsorption and desorption of H_2, N_2, and NH_3, thus, promoting NH_3 synthesis.

Table 3
Correlation of the reaction orders of NH_3 synthesis over the Ru/γ-Al_2O_3 and Cs-promoted Ru/γ-Al_2O_3 catalysts with the surface hydrogen and nitrogen residues.

Catalyst	h[a]	n[a]	a[a]	H_2/Ru (molar ratio)[b]	N_2/Ru (molar ratio)[b]
Ru/γ-Al_2O_3	0.2	1.0	–1.1	0.60 (322)	0.013 (426)
0.75Cs-Ru/γ-Al_2O_3	–0.6	0.9	–0.3	0.56 (295)	0.018 (397)
1.5Cs-Ru/γ-Al_2O_3	–0.3	0.9	–0.2	0.48 (292)	0.025 (371)
5Cs-Ru/γ-Al_2O_3	–0.4	0.9	–0.2	0.39 (242)	0.025 (364)

[a])Based on rate = $kP_{H2}{}^{h}P_{N2}{}^{n}P_{NH3}{}^{a}$. To minimize the reverse reaction, all data were measured at 430 °C and 1 MPa using a low catalyst mass (0.05 g), and the NH_3 yield was < 10% of the equilibrium yield. [b])Quantitatively analyzed by peak area in the temperature-programmed desorption-mass spectrometry profiles (Fig. 12). The numbers in parentheses represent the desorption temperatures at the peak maxima.

4. Conclusions

This study demonstrated that Cs-promoted Ru/γ-Al_2O_3 catalysts with Cs/Ru molar ratios of ~1.5 exhibited high performances and stabilities in low-pressure NH_3 synthesis, particularly under intermittent operation conditions. These results were comparable to those of recent studies of advanced Ru catalysts using advanced supports with improved electronic promotion effects. However, the promotion effects of the Cs-promoted Ru/γ-Al_2O_3 catalysts were significantly influenced by the structures of the active sites, which were influenced by the Cs/Ru molar ratios and changes in the surface acidity/basicity. Cs was first held at the acidic sites of γ-Al_2O_3 and then stuck to Ru boundaries as the Cs/Ru molar ratios were increased in the range of 0.5–1.5. Cs_2CO_3 formed under conditions of high Cs/Ru molar ratios (>1.5). Following the process of reductive activation, the metallic Ru particles and CsOH with reduced Cs species (i.e., CsOH-Cs^0/Ru active sites) were maximized at the Cs/Ru molar ratios of ~1.5, exhibiting high NH_3 synthesis activity. The DFT calculations revealed that CsOH reduced hydrogen poisoning due to hydrogen spillover and provided new active sites for NH_3 synthesis. In addition, the electronic promotion effect was observed when the reduced Cs species formed at the interfaces of the Ru and CsOH active sites, which was induced by hydrogen spillover. Results from kinetic analysis and temperature-programmed desorption studies revealed that the Cs^0/CsOH-Ru active sites of the Ru/γ-Al_2O_3 catalysts

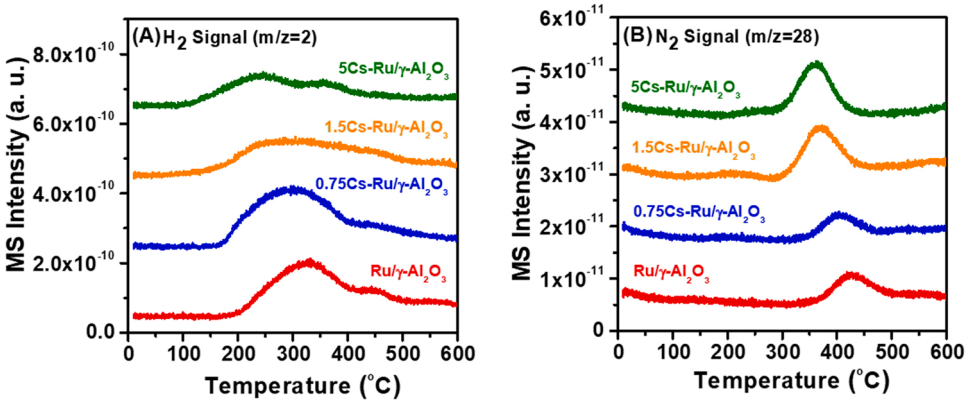

Fig. 12. Temperature-programmed desorption mass spectrometry profiles of the (A) H_2 signal, which was monitored using an m/z ratio of 2, and (B) N_2 signal, which was monitored using an m/z ratio of 28, over 0–5Cs-Ru/γ-Al_2O_3 after NH_3 synthesis at 400 °C and 0.1 MPa for 1 h. The H_2 and N_2 signals are normalized according to sample mass.

not only generated new active sites at the interfaces of the Ru particles and Cs^0/CsOH species but also altered the surface basicities/acidities, facilitating the adsorption and desorption of H_2, N_2, and NH_3. This, in turn, promoted the process of NH_3 synthesis. The Cs-promoted Ru/γ-Al_2O_3 catalysts with Cs/Ru molar ratios of ~1.5 are active, stable, and cost-efficient. Thus, they can be potentially used in industries for low-pressure NH_3 synthesis even under intermittent operation conditions. The results reported herein reveal the participation of the active sites of the alkali-promoted Ru-supported catalysts in the synthesis of NH_3, which findings are readily used for a wide range of hydrotreating reactions in industries. These catalysts can be potentially used to realize decarbonization during NH_3 synthesis in the presence of electrolytic hydrogen. Thus, the process of transformation of a fossil energy-based society to a low-carbon society can be accelerated.

CRediT authorship contribution statement

S.-Y. Chen designed the study, planned and conducted catalyst synthesis and characterization, conducted the TG-DTA and TPR/TPD/TPSR studies, wrote and revised the paper, supervised the study, and administered the project. / M. Nishi planned and conducted low-pressure ammonia synthesis and kinetic analysis/H. Tateno edited and revised the manuscript. / T. Mochizuki, H. Takagi, and T. Nanba edited and revised the manuscript and administered the project. C.-L. Chang conducted catalyst synthesis and characterization and the FE-SEM-EDS, HR-TEM, ICP-MS, and H_2-TPR-MS studies. / H.-H. Chou planned and supervised the study and administered the project. W.-C. Hsiao conducted the in situ XAS and data analysis. / C.-M. Yang planned and conducted the in situ XAS and data analysis, wrote and revised the manuscript, supervised the study, and administered the project. / Y. I. A. Reyes performed DFT calculations. / H.-Y. T. Chen planned and conducted the DFT calculations, wrote and revised the manuscript, supervised the study, and administered the project. ‡These authors contributed equally to this work.

Declaration of Competing Interest

The authors declare that they have no known competing financial interests or personal relationships that could have appeared to influence the work reported in this paper.

Acknowledgement

S.-Y. Chen, M. Nishi, H. Tateno, T. Mochizuki, H. Takagi, and T. Nanba acknowledge the AIST for financial support. C.-L. Chang and H.-H. Chou acknowledge the Ministry of Science and Technology (MOST), Taiwan, for financial support (MOST 110-2636-E-007-020; MOST 110-2622-8-007-015). W. -C. Hsiao and C.-M. Yang acknowledge MOST for financial support (MOST 109-2113-M-007-018-MY3 and 110-2113-M-007-023) and the Frontier Research Center on Fundamental and Applied Sciences of Matters from The Featured Areas Research Center Program within the framework of the Higher Education Sprout Project by the Ministry of Education (MOE) in Taiwan. Miss Ting-Yin Cheng and Miss Hsiang-Fang Chang at the Instrumentation Centre of National Tsing Hua University (MOST 110-2731-M-007-001) are also acknowledged for thermogravimetric analysis and ultramicrotomy, respectively. The National Synchrotron Radiation Research Centre (NSRRC), Taiwan, is gratefully acknowledged for XAS measurements. Y.I.A. Reyes and H.-Y. T. Chen acknowledge MOST (MOST 108-2112-M-007-023-MY3) and National Tsing Hua University (110Q2708E1 and 109Q2716E1), Taiwan, for their financial support. The computing resources were supported by TAIWANIA at the National Center for High-Performance Computing (NCHC) in Taiwan.

Appendix A. Supporting information

Supplementary data associated with this article can be found in the online version at doi:10.1016/j.apcatb.2022.121269.

References

[1] T. Kuramochi, Review of energy and climate policy developments in japan before and after fukushima, Renew. Sustain. Energy Rev. 43 (2015) 1320–1332.
[2] Y. Kikuchi, T. Ichikawa, M. Sugiyama, M. Koyama, Battery-Assisted low-cost hydrogen production from solar energy: rational target setting for future technology systems, Int. J. Hydrog. Energy 44 (2019) 1451–1465.
[3] F. Schüth, R. Palkovits, R. Schlögl, D.S. Su, Ammonia as a possible element in an energy infrastructure: catalysts for ammonia decomposition, Energy Environ. Sci. 5 (2012) 6278–6289.
[4] J. Cha, Y.S. Jo, H. Jeong, J. Han, S.W. Nam, K.H. Song, C.W. Yoon, Ammonia as an efficient cox-free hydrogen carrier: fundamentals and feasibility analyses for fuel cell applications, Appl. Energy 224 (2018) 194–204.
[5] H. Liu, Ammonia synthesis catalyst 100 years: practice, enlightenment and challenge, Chin. J. Catal. 35 (2014) 1619–1640.
[6] H.T. Oyama, S. Tamaru, F. Haber, Links between Japan and Germany in science and technology, Chem. Rec. 15 (2015) 535–549.
[7] K. Aika, Role of Alkali promoter in ammonia synthesis over ruthenium catalysts—effect on reaction mechanism, Catal. Today 286 (2017) 14–20.
[8] D.E. Brown, T. Edmonds, R.W. Joyner, J.J. McCarroll, S.R. Tennison, The genesis and development of the commercial bp doubly promoted catalyst for ammonia synthesis, Catal. Lett. 144 (2014) 545–552.
[9] Z. Kowalczyk, M. Krukowski, W. Raróg-Pilecka, D. Szmigiel, J. Zielinski, Carbon-based ruthenium catalyst for ammonia synthesis: role of the barium and caesium promoters and carbon support, Appl. Catal. A: Gen. 248 (2003) 67–73.
[10] D. Szmigiel, H. Bielawa, M. Kurtz, O. Hinrichsen, M. Muhler, W. Raróg, S. Jodzis, Z. Kowalczyk, L. Znak, J. Zieliński, The kinetics of ammonia synthesis over ruthenium-based catalysts: the role of barium and cesium, J. Catal. 205 (2002) 205–212.

[11] M. Nishi, S.-Y. Chen, H. Takagi, A. Mesoporous, Carbon-supported and Cs-promoted Ru catalyst with enhanced activity and stability for sustainable ammonia synthesis, ChemCatChem 10 (2018) 3411–3414.
[12] M. Nishi, S.-Y. Chen, H. Takagi, Energy efficient and intermittently variable ammonia synthesis over mesoporous carbon-supported Cs-Ru nanocatalysts, Catalysts 9 (2019) 406.
[13] M. Nishi, S.-Y. Chen, H. Takagi, Mild ammonia synthesis over ba-promoted ru/mpc catalysts: effects of the ba/ru ratio and the mesoporous structure, Catalysts 9 (2019) 480.
[14] M. Nishi, S.-Y. Chen, H. Takagi, X-ray absorption spectroscopy of Ba- and Cs-promoted ru/mesoporous carbon catalysts for long-term ammonia synthesis under intermittent operation conditions, Sustain. Energy Fuels 4 (2020) 832–842.
[15] S.-Y. Chen, M. Nishi, A. Chang, W.-C. Hsiao, T. Mochizuki, H. Takagi, C.-M. Yang, Well-ordered Cs–Ru/@SBA-15 nanocomposite materials for low pressure ammonia synthesis. Sustain. Energy Fuels 4 (2020) 5802–5811.
[16] C.N. Satterfield, Heterogeneous Catalysis in Industrial Practice, McGraw-Hill, 1991.
[17] H. Wang, R. Prins, Hydrodesulfurization of dibenzothiophene, 4,6-dimethyldibenzothiophene, and their hydrogenated intermediates over Ni–MoS_2/γ-Al_2O_3, J. Catal. 264 (2009) 31–43.
[18] Y. Sun, R. Prins, Mechanistic studies and kinetics of the hydrodesulfurization of dibenzothiophene on Co–MoS_2/γ–Al_2O_3, J. Catal. 267 (2009) 193–201.
[19] S.-Y. Chen, M. Nishi, T. Mochizuki, H. Takagi, A. Takatsuki, W. Roschat, M. Toba, Y. Yoshimura, Co-processing of jatropha-derived bio-oil with petroleum distillates over mesoporous como and nimo sulfide catalysts, Catalysts 8 (2018) 59.
[20] S.Y. Chen, T. Mochizuki, M. Nishi, H. Takagi, Y. Yoshimura, M. Toba, Hydrotreating of jatropha-derived bio-oil over mesoporous sulfide catalysts to produce drop-in transportation fuels, Catalysts 9 (2019) 392.
[21] K. Aika, H. Hori, A. Ozaki, Activation of nitrogen by alkali metal promoted transition metal I. Ammonia synthesis over ruthenium promoted by alkali metal, J. Catal. 27 (1972) 424–431.
[22] S. Murata, K. Aika, Preparation and characterization of chlorine-free ruthenium catalysts and the promoter effect in ammonia synthesis: 1. An alumina-supported ruthenium catalyst, J. Catal. 136 (1992) 110–117.
[23] S. Murata, K. Aika, Preparation and characterization of chlorine-free ruthenium catalysts and the promoter effect in ammonia synthesis: 2. A lanthanide oxide-promoted Ru/Al_2O_3 catalyst, J. Catal. 136 (1992) 118–125.
[24] A. Miyazaki, I. Balint, K. Aika, Y. Nakano, Preparation of high activity catalyst for ammonia synthesis by supporting well-defined ru nanoparticles on γ-Al_2O_3, Chem. Lett. 30 (2001) 1332–1333.
[25] A. Miyazaki, I. Balint, K. Aika, Y. Nakano, Preparation of Ru nanoparticles supported on γ-Al_2O_3 and its novel catalytic activity for ammonia synthesis, J. Catal. 204 (2001) 364–371.
[26] Y.V. Larichev, B.L. Moroz, E.M. Moroz, V.I. Zaikovskii, S.M. Yunusov, E. S. Kalyuzuhnaya, V.B. Shur, V.I. Bukhtiyarov, Effect of the support on the nature of metal-promoter interactions in Ru-Cs^+/MgO and Ru-Cs^+/Al_2O_3 catalysts for ammonia synthesis, Kinet. Catal. 46 (2005) 891–899.
[27] K. Aika, K. Shimazaki, Y. Hattori, A. Ohya, S. Ohshima, K. Shirota, A. Ozaki, Support and promot effect of ruthenium catalyst, J. Catal. 92 (1985) 296–304.
[28] T. Hikita, Y. Kadowaki, K. Aika, Promoter action of alkali nitrate in raney ruthenium catalyst for activation of nitrogen, J. Phys. Chem. 91 (1991) 3396–9402.
[29] K. Aika, T. Takano, S. Murata, Preparation and characterization of chlorine-free ruthenium catalysts and the promoter effect in ammonia synthesis 3. A magnesia-supported ruthenium catalyst, J. Catal. 136 (1992) 126–140.
[30] W. Raróg-Pilecka, E. Miskiewicz, S. Jodzis, J. Petryk, D. Łomot, Z. Kaszkur, Z. Karpiński, Z. Kowalczyk, Carbon-supported ruthenium catalysts for NH_3 synthesis doped with caesium nitrate: activation process, working state of Cs–Ru/C, J. Catal. 239 (2006) 313–325.
[31] K. Honkala, A. Hellman, I.N. Remediakis, A. Logadottir, A. Carlsson, S. Dahl, C. H. Christensen, J.K. Nørskov, Ammonia synthesis from first principles calculations, Science 307 (2005) 555–558.
[32] A. Hellman, E.J. Baerends, M. Biczysko, T. Bligaard, C.H. Christensen, D.C. Clary, S. Dahl, van R. Harrevelt, K. Honkala, H. Jonsson, G.J. Kroes, M. Luppi, U. Manthe, J.K. Nørskov, R.A. Olsen, J. Rossmeisl, E. Skúlason, C.S. Tautermann, A.J. C. Varandas, J.K. Vincent, Predicting catalysis: understanding ammonia synthesis from first-principles calculations, J. Phys. Chem. B 110 (2006) 17719–17735.
[33] B. Lin, L. Heng, B. Fang, H. Yin, J. Ni, X. Wang, J. Lin, L. Jiang, Ammonia synthesis activity of alumina-supported ruthenium catalyst enhanced by alumina phase transformation, ACS Catal. 9 (2019) 1635–1644.
[34] M. Hara, M. Kitano, H. Hosono, Ru-Loaded $C_{12}A_7$: e^- electride as a catalyst for ammonia synthesis, ACS Catal. 7 (2017) 2313–2324.
[35] K. Sato, K. Imamura, Y. Kawano, S. Miyahara, T. Yamamoto, S. Matsumura, K. Nagaoka, A low-crystalline ruthenium nano-layer supported on praseodymium oxide as an active catalyst for ammonia synthesis, Chem. Sci. 8 (2017) 674–679.
[36] W. Li, P. Liu, R. Niu, J. Li, S. Wang, Influence of CeO_2 supports prepared with different precipitants over Ru/CeO_2 catalysts for ammonia synthesis, Solid State Sci. 99 (2020), 105983.
[37] World's First Successful Ammonia Synthesis Using Renewable Energy-Based Hydrogen and Power Generation. ⟨https://fuelcellsworks.com/news/worlds-first-successful-ammonia-synthesis-using-renewable-energy-based-hydr/⟩ (Accessed 2018-10).
[38] R. Javaid, H. Matsumoto, T. Nanba, Influence of Reaction conditions and promoting role of ammonia produced at higher temperature conditions in its synthesis process over Cs-Ru/MgO catalyst, ChemistrySelect 4 (2019) 2218–2224.
[39] R. Javaid, T. Nanba, $MgFe_2O_4$-supported Ru catalyst for ammonia synthesis: promotive effect of chlorine, ChemistrySelect 5 (2020) 4312–4315.
[40] R. Javaid, T. Nanba, Effect of reaction conditions and surface characteristics of Ru/CeO_2 on catalytic performance for ammonia synthesis as a clean fuel, Int. J. Hydrog. Energy 46 (2021) 18107–18115.
[41] Y. Manaka, Y. Nagata, K. Kobayashi, D. Kobayashi, T. Nanba, The effect of a ruthenium precursor on the low-temperature ammonia synthesis activity over Ru/CeO_2, Dalton Trans. 49 (2020) 17143–17146.
[42] R. Javaid, Y. Aoki, T. Nanba, Highly efficient $Ru/MgO–Er_2O_3$ catalysts for ammonia synthesis, J. Phys. Chem. Solids 146 (2020), 109570.
[43] T. Nanba, Y. Nagata, K. Kobayashi, R. Javaid, R. Atsumi, M. Nishi, T. Mochizuki, Y. Manaka, H. Kojima, T. Tsujimura, H. Matsumoto, T. Fujimoto, K. Suzuki, T. Oouchi, S. Kameda, Y. Hoshino, S. Fujimoto, M. Kai, Y. Fujimura, Explorative study of a Ru/CeO_2 catalyst for NH_3 synthesis from renewable hydrogen and demonstration of NH_3 synthesis under a range of reaction conditions, J. Jpn. Pet. Inst. 64 (2021) 1–9.
[44] B. Ravel, M. Newville, ATHENA, ARTEMIS, HEPHAESTUS: Data Analysis for X-ray Absorption Spectroscopy using IFEFFIT, J. Synchro. Radiat. 12 (2005) 537–541.
[45] G. Kresse, J. Furthmüller, Efficient iterative schemes for ab initio total-energy calculations using a plane-wave basis set, Phys. Rev. B 54 (1996) 11169.
[46] G. Kresse, J. Furthmüller, Efficiency of Ab-initio total energy calculations for metals and semiconductors using a plane-wave basis set, Comput. Mater. Sci. 6 (1996) 15–50.
[47] G. Kresse, J. Hafner, Ab initio molecular dynamics for liquid metals, Phys. Rev. B 47 (1993) 558.
[48] P.E. Blöchl, Projector augmented-wave method, Phys. Rev. B 50 (1994) 17953.
[49] G. Kresse, D. Joubert, From ultrasoft pseudopotentials to the projector augmented-wave method, Phys. Rev. B 59 (1999) 1758.
[50] J.P. Perdew, K. Burke, M. Ernzerhof, Generalized gradient approximation made simple, Phys. Rev. Lett. 77 (1996) 3865.
[51] H.J. Monkhorst, J.D. Pack, Special points for brillouin-zone integrations, Phys. Rev. B 13 (1976) 5188.
[52] W. Tang, E. Sanville, G. Henkelman, A grid-based bader analysis algorithm without lattice bias, J. Phys. Condens. Matter 21 (2009), 084204.
[53] E. Sanville, S.D. Kenny, R. Smith, G. Henkelman, Improved grid-based algorithm for bader charge allocation, J. Comput. Chem. 28 (2007) 899–908.
[54] S.-Y. Chen, L. Attanatho, A. Chang, T. Laosombut, M. Nishi, T. Mochizuki, H. Takagi, C.-M. Yang, Y. Abe, M. Toba, N. Chollacoop, Y. Yoshimura, Profiling and catalytic upgrading of commercial palm oil-derived biodiesel fuels for high-blend fuels, Catal. Today 332 (2019) 122–131.
[55] S.-Y. Chen, A. Chang, A.N. Rungsi, L. Attanatho, C.-L. Chang, J.-H. Pan, A. Suemanotham, T. Takagi, H. Mochizuki, C.-M. Yang, A. Luengnarumitchai, H.-H. Chou, Superficial Pd nanoparticles supported on carbonaceous SBA-15 as efficient hydrotreating catalyst for upgrading biodiesel fuel, Appl. Catal. A: Gen. 602 (2020), 117707.
[56] F. Su, F.Y. Lee, L. Lv, J. Liu, X.N. Tian, X.S. Zhao, Sandwiched ruthenium/carbon nanostructures for highly active heterogeneous hydrogenation, Adv. Funct. Mater. 17 (2007) 1926–1931.
[57] S. Wu, Y.-K. Peng, T.-Y. Chen, J. Mo, A. Large, I. McPherson, H.-L. Chou, I. Wilkinson, F. Venturini, D. Grinter, P.F. Escorihuela, G. Held, S.C.E. Tsang, Removal of hydrogen poisoning by electrostatically polar MgO support for low-pressure NH_3 synthesis at a high rate over the Ru catalyst, ACS Catal. 10 (2020) 5614–5622.
[58] B. Lin, Y. Liu, L. Heng, X. Wang, J. Ni, J. Lin, L. Jiang, Morphology effect of ceria on the catalytic performances of Ru/CeO_2 Catalysts for ammonia synthesis, Ind. Eng. Chem. Res. 57 (2018) 9127–9135.
[59] Y. Wu, C. Li, B. Fang, X. Wang, J. Ni, B. Lin, J. Lin, L. Jiang, Enhanced ammonia synthesis performance of ceria-supported Ru catalysts via introduction of titanium, Chem. Comm. 56 (2020) 1141–1144.
[60] X. Wang, L. Li, Z. Fang, Y. Zhang, J. Ni, B. Lin, L. Zheng, C. Au, L. Jiang, Atomically dispersed Ru catalyst for low-temperature nitrogen activation to ammonia via an associative mechanism, ACS Catal. 10 (2020) 9504–9514.
[61] M. Kitano, Y. Inoue, M. Sasase, K. Kishida, Y. Kobayashi, K. Nishiyama, T. Tada, S. Kawamura, T. Yokoyama, M. Hara, H. Hosono, Self-organized ruthenium–barium core–shell nanoparticles on a mesoporous calcium amide matrix for efficient low-temperature ammonia synthesis, Angew. Chem. 130 (2018) 2678–2682.
[62] M. Hattori, T. Mori, T. Arai, Y. Inoue, M. Sasase, T. Tada, M. Kitano, T. Yokoyama, M. Hara, H. Hosono, Enhanced catalytic ammonia synthesis with transformed BaO, ACS Catal. 8 (2018) 10977–10984.
[63] K. Sato, S. Miyahara, Y. Ogura, K. Tsujimaru, Y. Wada, T. Toriyama, T. Yamamoto, S. Matsumura, K. Nagaoka, Surface dynamics for creating highly active Ru sites for ammonia synthesis: accumulation of a low-crystalline, oxygen-deficient nanofraction, ACS Sustain. Chem. Eng. 8 (2020) 2726–2734.
[64] K. Sato, K. Nagaoka, Boosting ammonia synthesis under mild reaction conditions by precise control of the basic oxide–Ru interface, Chem. Lett. 50 (2021) 687–696.
[65] W. Raróg-Pilecka, E. Miśkiewicz, D. Szmigiel, Z. Kowalczyk, Structure sensitivity of ammonia synthesis over promoted ruthenium catalysts supported on graphitised carbon, J. Catal. 231 (2005) 11–19.
[66] D. Szmigiel, H. Bielawa, M. Kurtz, O. Hinrichsen, M. Muhler, W. Raróg, S. Jodzis, Z. Kowalczyk, L. Znak, J. Zieliński, The kinetics of ammonia synthesis over ruthenium-based catalysts: the role of barium and cesium, J. Catal. 205 (2002) 205–212.
[67] J. Folke, K. Dembélé, F. Girgsdies, H. Song, R. Eckert, S. Reitmeier, A. Reitzmann, R. Schlögl, T. Lunkenbein, H. Ruland, Promoter effect on the reduction behavior of

wuestite-based catalysts for ammonia synthesis, Catal. Today (2021) (https://doi.org/10.1016/j.cattod.2021.03.013).
[68] W. Karim, C. Spreafico, A. Kleibert, J. Gobrecht, J. VandeVondele, Y. Ekinci, A. van, J. Bokhoven, Catalyst support effects on hydrogen spillover, Nature 541 (2017) 68–71.
[69] I. Arčon, A. Kodre, J.P. Gomilšek, M. Hribar, A. Mihelič, Cs L-Edge EXAFS atomic absorption background, Phys. Scr. 2005 (2005) 235–236.
[70] R. Qin, L. Zhou, P. Liu, Y. Gong, K. Liu, C. Xu, Y. Zhao, L. Gu, G. Fu, N. Zheng, Alkali ions secure hydrides for catalytic hydrogenation, Nat. Catal. 3 (2020) 703–709.
[71] I. Rossetti, L. Sordelli, P. Ghigna, S. Pin, M. Scavini, L. Forni, EXAFS-XANES evidence of in situ cesium reduction in Cs-Ru/C catalysts for ammonia synthesis, Inorg. Chem. 50 (2011) 3757–3765.
[72] K.L. Eslava, A. Lglesias-Juez, G. Agostini, M. Fernandez-Garcia, A. Guerrero-Ruiz, I. Rodriguez-Ramos, Time-resolved XAS Investigation of the local environment and evolution states of a fischer–tropsch Ru–Cs/C catalyst, ACS Catal. 6 (2016) 1437–1445.
[73] J.J. Mortensen, Y. Morikawa, B. Hammer, J.K. Nørskov, Density functional calculations of N_2 adsorption and dissociation on a Ru(0001) surface, J. Catal. 169 (1997) 85–92.
[74] J.J. Mortensen, B. Hammer, J.K. Nørskov, Alkali promotion of N_2 dissociation over Ru(0001), Phys. Rev. Lett. 80 (1998) 4333–4336.
[75] Y. Kadowaki, K. Aika, Promoter effect of Sm_2O_3 on $RuAl_2O_3$ in ammonia synthesis, J. Catal. 161 (1996) 178–185.
[76] M. Itoh, M. Saito, C.Y. Li, J. Iwamoto, K. Machida, High dependence for reaction pressure on Ru/(MgO-CeO_2)/Ag-Pd ammonia synthesis membrane reactor, Chem. Lett. 34 (2005) 1104–1105.
[77] B. Lin, K. Wei, X. Ma, M. Jianxin, Study of potassium promoter effect for Ru/AC catalysts for ammonia synthesis, Catal. Sci. Technol. 3 (2013) 1367–1374.
[78] K. Imamuraa, S.-I. Miyahara, Y. Kawano, K. Sato, Y. Nakasaka, K. Nagaoka, Kinetics of ammonia synthesis over Ru/Pr2O3, J. Taiwan Inst. Chem. Eng. 105 (2019) 50–56.